

Store-Operated Ca^{2+} Entry in Sensory Neurons: Functional Role and the Effect of Painful Nerve Injury

Geza Gemes,^{1,2} Madhavi Latha Yadav Bangaru,¹ Hsiang-En Wu,¹ Qingbo Tang,¹ Dorothee Weihrauch,¹ Andrew S. Koopmeiners,¹ James M. Cruikshank,¹ Wai-Meng Kwok,¹ and Quinn H. Hogan^{1,3}

¹Department of Anesthesiology, Medical College of Wisconsin, Milwaukee, Wisconsin 53226, ²Department of Anesthesiology and Intensive Care Medicine, Medical University of Graz, 8036 Graz, Austria, and ³Zablocki Veterans Affairs Medical Center, Milwaukee, Wisconsin 53295

Painful nerve injury disrupts levels of cytoplasmic and stored Ca^{2+} in sensory neurons. Since influx of Ca^{2+} may occur through store-operated Ca^{2+} entry (SOCE) as well as voltage- and ligand-activated pathways, we sought confirmation of SOCE in sensory neurons from adult rats and examined whether dysfunction of SOCE is a possible pathogenic mechanism. Dorsal root ganglion neurons displayed a fall in resting cytoplasmic Ca^{2+} concentration when bath Ca^{2+} was withdrawn, and a subsequent elevation of cytoplasmic Ca^{2+} concentration (40 ± 5 nM) when Ca^{2+} was reintroduced, which was amplified by store depletion with thapsigargin ($1 \mu\text{M}$), and was significantly reduced by blockers of SOCE, but was unaffected by antagonists of voltage-gated membrane Ca^{2+} channels. We identified the underlying inwardly rectifying Ca^{2+} -dependent I_{CRAC} (Ca^{2+} release activated current), as well as a large thapsigargin-sensitive inward current activated by withdrawal of bath divalent cations, representing SOCE. Molecular components of SOCE, specifically STIM1 and Orai1, were confirmed in sensory neurons at both the transcript and protein levels. Axonal injury by spinal nerve ligation (SNL) elevated SOCE and I_{CRAC} . However, SOCE was comparable in injured and control neurons when stores were maximally depleted by thapsigargin, and STIM1 and Orai1 levels were not altered by SNL, showing that upregulation of SOCE after SNL is driven by store depletion. Blockade of SOCE increased neuronal excitability in control and injured neurons, whereas injured neurons showed particular dependence on SOCE for maintaining levels of cytoplasmic and stored Ca^{2+} , which indicates a compensatory role for SOCE after injury.

Introduction

The concentration of cytoplasmic Ca^{2+} ($[\text{Ca}^{2+}]_c$) is the dominant regulator of numerous neuronal functions, including differentiation, excitation, synaptic transmission, and apoptosis (Ghosh and Greenberg, 1995; Paschen, 2001). Sensory neurons possess an array of plasmalemmal channels that admit Ca^{2+} in response to depolarization, binding of ligands, heat, cold, depressed pH, and mechanical distortion. Ca^{2+} signals initiated by these high-conductance channels are modulated by concurrent extrusion of Ca^{2+} from the neuron, as well as bidirectional exchange of Ca^{2+} between the neuronal cytoplasm and stores in endoplasmic reticulum (ER) and mitochondria. Inflammation and injury of sensory neurons disrupts this ensemble of interacting processes (Fuchs et al., 2007; Lu and Gold, 2008; Gemes et al., 2009; Rigaud et al., 2009).

There is expanding recognition in diverse cell types of Ca^{2+} entry through low-conductance plasmalemmal channels that are regulated by the level of Ca^{2+} stored in the ER, a process known as store-operated Ca^{2+} entry (SOCE). This pathway and its underlying Ca^{2+} -release-activated current, I_{CRAC} , are well defined

in nonexcitable cells (Hofer et al., 1998; Braun et al., 2001; Mercer et al., 2006), for which SOCE is the dominant route of Ca^{2+} influx. Recent identification of stromal interaction molecule 1 (STIM1) as the ER Ca^{2+} sensor that regulates SOCE (Stathopulos et al., 2006), and Orai1 as a pore-forming subunit conducting I_{CRAC} (Mercer et al., 2006), has allowed detailed characterization of SOCE in cells expressing these collaborating elements. Such studies have established cardinal features of SOCE, including amplification by depletion of Ca^{2+} stores, inward rectification of I_{CRAC} , high inward conductance of Na^+ through store-operated Ca^{2+} channels in the absence of divalent cations (DeHaven et al., 2007), and sensitivity of SOCE to certain semiselective blockers (Putney, 2001).

A small number of studies have examined SOCE in neurons. Interference with SOCE may depress $[\text{Ca}^{2+}]_c$ and deplete sensory neuron intracellular Ca^{2+} stores (Usachev and Thayer, 1999), which also follows painful nerve injury (Rigaud et al., 2009). Additionally, SOCE may regulate kinase activity and synaptic transmission (Emptage et al., 2001; Cohen and Fields, 2006), providing strong motivation for expanded exploration of SOCE in sensory neurons under baseline and injured conditions. Accordingly, the present study pursues several goals. First, since previous findings that identified the basic effects of SOCE on resting $[\text{Ca}^{2+}]_c$ and Ca^{2+} stores in sensory neurons examined neonatal sensory neurons after prolonged culture (Usachev and Thayer, 1999), we sought to extend those findings using acutely isolated adult sensory neurons, to limit effects of prolonged culture (Scott and Edwards, 1980) and to allow comparison in pain

Received Sept. 26, 2010; revised Dec. 19, 2010; accepted Dec. 29, 2010.

This work was supported by National Institutes of Health Grants NS-42150 (Q.H.H.) and DA-K01 02475 (H.-E.W.). We thank Dr. Ranjan K. Dash (Department of Physiology, Biotechnology, and Bioengineering Center, Medical College of Wisconsin) for expert assistance.

Correspondence should be addressed to Dr. Quinn H. Hogan, Department of Anesthesiology, Medical College of Wisconsin, 8701 Watertown Plank Road, Milwaukee, WI 53226. E-mail: qhogan@mcw.edu.

DOI:10.1523/JNEUROSCI.5053-10.2011

Copyright © 2011 the authors 0270-6474/11/313536-14\$15.00/0

models using adult animals. Second, we wanted to determine the fundamental features of SOCE in sensory neurons by directly examining I_{CRAC} and determining whether these neurons express the molecular components of SOCE described in other cell types. Third, since the functional role of SOCE is poorly defined in neurons, we examined the influence of SOCE on Ca^{2+} stores, resting $[\text{Ca}^{2+}]_c$, and excitability. Finally, to determine whether SOCE contributes to neuropathic pain, we also characterized SOCE in a model of peripheral nerve injury.

Materials and Methods

All methods and use of animals were approved by the Medical College of Wisconsin Institutional Animal Care and Use Committee.

Injury model. Male Sprague Dawley (Taconic Farms) rats weighing 160–180 g were subjected to spinal nerve ligation (SNL) in a manner derived from the original technique (Kim and Chung, 1992). Rats were anesthetized with 2% isoflurane in oxygen and the right paravertebral region was exposed. After removal of the sixth lumbar (L6) transverse process, the L5 and L6 spinal nerves were ligated with 6-0 silk suture and transected distal to the ligation. The fascia was closed with 4-0 resorbable polyglactin suture and the skin closed with staples. Control animals received anesthesia, skin incision, and stapling only. After surgery, the rats were returned to their cages and kept under normal housing conditions with access to pellet food and water *ad libitum*.

Sensory testing. Rats underwent sensory testing for a form of hyperalgesic behavior that we have previously documented to be associated with an aversive percept (Hogan et al., 2004; Wu et al., 2010). Briefly, on three different days between 10 and 17 d after surgery, right plantar skin was mechanically stimulated with a 22 gauge spinal needle with adequate pressure to indent but not penetrate the skin. Whereas control animals respond with only a brief reflexive withdrawal, rats after SNL may display a complex hyperalgesia response that incorporates sustained licking, chewing, grooming, and sustained elevation of the paw. The frequency of hyperalgesia responses was tabulated for each rat.

Neuron isolation and plating. The right L5 ganglia were rapidly harvested after isoflurane anesthesia and decapitation and were incubated in 0.01% blendzyme 2 (Roche Diagnostics) for 30 min followed by incubation in 0.25% trypsin (Sigma-Aldrich) and 0.125% DNase (Sigma-Aldrich) for 30 min, both dissolved in DMEM/F12 with glutamax (Invitrogen). After exposure to 0.1% trypsin inhibitor and centrifugation, the pellet was gently triturated in culture medium containing Neural Basal Media A with B27 supplement (Invitrogen), 0.5 mM glutamine, 10 ng/ml nerve growth factor 7S (Alomone Labs), and 0.02 mg/ml gentamicin (Invitrogen). Dissociated neurons were plated onto poly-L-lysine-coated glass coverslips (Deutsches Spiegelglas; Carolina Biological Supply) and maintained at 37°C in humidified 95% air and 5% CO_2 for 2 h, and were studied no later than 6 h after harvest.

Solutions and agents. Unless otherwise specified, the bath contained Tyrode's solution (in mM: 140 NaCl, 4 KCl, 2 CaCl_2 , 10 glucose, 2 MgCl_2 , 10 HEPES, with an osmolality of 297–300 mOsm and pH 7.40). In some experiments, a Ca^{2+} -free Tyrode's was used that contained the following (in mM): 140 NaCl, 4 KCl, 10 glucose, 2 MgCl_2 , 10 HEPES, and 0.2 EGTA.

Agents were obtained as follows: 2-aminoethyl diphenylborinate (2-APB), bovine albumin, caffeine, dimethylsulfoxide (DMSO), lanthanum chloride, 1-[2-(4-methoxyphenyl)-2-[3-(4-methoxyphenyl)propoxy]ethyl]imidazole (SKF-96365), thapsigargin (TG), N,N,N',N' -tetrakis(2-pyridylmethyl)-ethylenediamine (TPEN), and 7-nitroindazole (7-NI) from Sigma-Aldrich, fura-2 AM from Invitrogen, and 1-(2-trifluoromethylphenyl)imidazole (TRIM) from Alexis Biochemicals. Stock solutions of 2-APB, SKF-96365, TG, 7-NI, TRIM, and fura-2 AM were dissolved in DMSO and subsequently diluted in the relevant bath solution such that final bath concentration of DMSO was 0.2% or less, which has no effect on $[\text{Ca}^{2+}]_c$ ($n = 20$) (data not shown). The 0.5 ml recording chamber was constantly superfused by a gravity-driven bath flow at a rate of 3 ml/min. Agents were delivered by directed microperfusion controlled by a computerized valve system through a 500- μm -diameter hollow quartz fiber 300 μm upstream from the neurons. This flow completely displaced the bath solution, and constant flow was maintained by delivery of bath solution

when specific agents were not being administered. Solution changes were achieved within 200 ms.

Measurement of cytoplasmic Ca^{2+} concentration. Coverslips holding plated neurons were transferred to a room temperature 5 μM solution of fura-2 AM that contained 2% bovine albumin to aid dispersion of the fluorophore. After 30 min, they were washed three times with regular Tyrode's solution and left in a dark environment for deesterification for 30 min and then mounted onto the recording chamber. The fluorophore was excited alternately with 340 and 380 nm wavelength illumination (150 W xenon, Lambda DG-4; Sutter), and images were acquired at 510 nm using a cooled 12 bit digital camera (Coolsnap fx; Photometrics) and inverted microscope (Diaphot 200; Nikon Instruments) through a 20 or 40 \times Fluor oil-immersion objective. Recordings from each neuron were obtained as separate regions of interest by appropriate software (Meta-Fluor; Molecular Devices) at a rate of 3 Hz. After background subtraction, the fluorescence ratio R for individual neurons was determined as the intensity of emission during 340 nm excitation (I_{340}) divided by I_{380} on a pixel-by-pixel basis. The calcium concentration was then estimated by the formula $[\text{Ca}^{2+}]_c = K_d \cdot \beta \cdot (R - R_{\text{min}})/(R_{\text{max}} - R)$, where $\beta = (I_{380\text{max}})/I_{380\text{min}}$. Values of R_{min} , R_{max} , and β were determined by periodical *in situ* calibrations as described previously (Fuchs et al., 2005) and were 0.38, 8.49, and 9.54, respectively, and 224 nm was used as K_d (Gryniewicz et al., 1985). Neurons were visually examined in the bright-field mode and those showing signs of lysis, crenulation, or superimposed glial cells were excluded. Similarly, only neurons with stable baseline R traces were further evaluated. Traces were analyzed using Axograph X 1.1 (Axograph Scientific). Neurons were characterized by diameter as large ($>34 \mu\text{m}$), which represent predominantly fast-conducting non-nociceptive $A\beta$ neurons, or small ($<34 \mu\text{m}$), which represent a mix of $A\beta$ neurons, slower conducting $A\delta$ nociceptive neurons, and C-type nonmyelinated nociceptive neurons (data not shown). Unless otherwise stated, small neurons were examined. Fura-2 fluorescence during Sr^{2+} entry represents a mix of cytoplasmic Ca^{2+} and Sr^{2+} , and transients were not calibrated, but rather are reported in R units.

Quantitative reverse transcriptase-PCR analysis. Total RNA was isolated from the homogenized L5 dorsal root ganglia (DRGs) of control animals, and separately from the L4 and L5 DRGs of SNL rats harvested 21 d after surgery, following the manufacturer's (Invitrogen) instructions using Trizol reagent (from aqueous phase). After DNase treatment, cDNA was synthesized from equal amounts of RNA using SuperScript III first-strand synthesis kit (Invitrogen). Real-time PCR analysis was performed in duplicate for each run using iQ SYBR Green supermix (Bio-Rad) and specific primers to quantify the cDNA levels of STIM1 [forward primer (FP), GTGCGCTCGTCTTGCCCTGT; reverse primer (RP), TGCGGACGGCTCAAAGAGCTG] and Orai1 (FP, CTGGCGCAAGCTCTACTTGA; RP, AGTAACCTGGCGGGTAGTC). The expression level of housekeeping gene *Tubb5* (FP, CATGGACGAGATGGAGTTCA; RP, GAAA-CAAAGGGCAGTTGGAA) was used for normalization. For each sample, two interrater determinations were averaged. Statistical evaluation was performed on normalized values. Figures show fold difference in expression of STIM1 and Orai1 in the DRGs from SNL animals, which was calculated by comparison with that of control DRGs.

Immunoblotting. Total protein was isolated from homogenized L5 DRGs from control animals and separately from L4 and L5 DRGs of SNL rats harvested 21 d after surgery following manufacturer's (Invitrogen) instructions using Trizol reagent and sequential precipitation (from organic phase). Equal amounts of protein (20–50 μg ; determined by Pierce bicinchoninic acid protein assay kit; Thermo Scientific) were separated on 4–15% SDS-PAGE gel (Bio-Rad) and transferred onto a polyvinylidene fluoride membrane. After blocking with 5% milk in TBST (Tris-buffered saline plus 0.1% Tween 20), blots were sequentially probed with anti- β -Tubulin I mouse monoclonal antibody (1:20,000; Sigma-Aldrich; catalog #T7816), anti-STIM1 rabbit polyclonal antibody (1:500; ProSci; catalog #4119), and anti-Orai1 rabbit polyclonal antibody (1:1000; ProSci; catalog #4281). Because of nonspecific bands using this antibody, Orai1 protein expression was examined with a second anti-Orai1 rabbit polyclonal antibody (1:1000; Abcam), which also showed nonspecific binding. The ProSci antibody was used for data shown here. Western blot Restore stripping buffer (Thermo Scientific) was used to strip antibodies

from the membrane. Horseradish peroxidase-conjugated goat anti-rabbit and goat anti-mouse antibodies (1:2000) were used as secondary antibodies (Pierce). Enhanced chemiluminescence (GE Healthcare) was used for the detection of the protein bands. The bands obtained were quantified using NIH ImageJ program, and β -Tubulin I was used to normalize the protein loading.

Immunohistochemistry. Twenty-one days after surgery, control and injured rats were perfused with saline followed by 4% paraformaldehyde. The control L5 DRGs and L4 and L5 DRGs from SNL rats were harvested and postfixed in 4% paraformaldehyde overnight, followed by incubation in 30% sucrose for 8 h. Tissues were frozen in TissueTek optimal cutting temperature compound (Ted Pella). Sections (15 μm) were permeabilized with PBS plus 0.1% Triton X-100 (PBST) for 20 min, blocked with 8% normal goat serum for 2 h, and then incubated overnight with anti-STIM1 rabbit polyclonal antibody (1:1500; ProSci). After three washes with PBST, sections were incubated with Alexa Fluor 568 goat anti-rabbit antibody (1:500; Invitrogen) for 1 h. The sections were washed thrice with PBST and examined by confocal microscopy. The expression level of STIM1 protein was represented by the average image intensity of two sites in each cell in images that were captured using standardized camera parameters, and cell area was determined by outlining the neuronal profile.

To determine colocalization of STIM1 with the neuron-specific nuclear protein (NeuN), sections were blocked with 8% NGS, incubated overnight with anti-STIM1 rabbit polyclonal antibody (1:1500) and anti-NeuN mouse monoclonal antibody (1:500; Millipore) followed by incubation with Alexa Fluor 568 anti-rabbit IgG (1:500; Invitrogen) for STIM1 antibody and Alexa Fluor 488 goat anti-mouse IgG conjugated with (1:1000; Invitrogen) to bind NeuN antibody for 1 h. To determine colocalization of STIM1 with glutamine synthetase, sections were blocked with 8% NGS, incubated overnight with anti-STIM1 rabbit polyclonal antibody (1:1500) followed by incubation with Alexa Fluor 568 goat anti-rabbit IgG (1:500) (Invitrogen). After three washes with PBST, the sections were incubated with anti-glutamine synthetase rabbit polyclonal antibody (1:500) (Santa Cruz Biotechnology) for 2 h. After washes, sections were incubated with Alexa Fluor 488 goat anti-rabbit IgG (1:1000; Invitrogen) for 1 h. Sections were washed three times with PBST and examined by confocal microscopy.

Intracellular electrophysiological recording. Intracellular recordings were performed with microelectrodes fashioned from borosilicate glass (1 mm outer diameter, 0.5 mm inner diameter; with Omega fiber; FHC) using a P-97 programmable micropipette puller (Sutter). Pipettes were filled with 2 M potassium acetate, which was buffered with 10 mM HEPES, with a resulting resistance of 70–100 M Ω . For recording from dissociated neurons, coverslips carrying the neurons were mounted onto a 500 μl chamber and constantly superfused with Tyrode's solution at 3 ml/min. Neurons were selected in bright-field mode on an upright microscope using a 40 \times water-immersion objective and impaled under direct vision with the aid of an oscillating current to the recording electrode. Membrane potential was recorded using an active bridge amplifier (Axoclamp 2B; Molecular Devices). Voltage recordings were filtered at 10 kHz and then digitized at 40 kHz (Digidata 1322A; Molecular Devices; and Axograph X 1.1) for data acquisition and analysis. Alternatively, for recording from neuronal somata in intact DRGs, ganglia were perfused with a bath solution (in mM: 128 NaCl, 3.5 KCl, 1.2 MgCl₂, 2.3 CaCl₂, 1.2 NaH₂PO₄, 24.0 NaHCO₃, 11.0 glucose) bubbled by 5% CO₂ and 95% O₂ to maintain a pH of 7. Neurons were impaled using differential interference contrast imaging with infrared illumination. Voltage error was minimized using a switching amplifier (Axoclamp 2B) operating in discontinuous current-clamp mode with a switching rate of 2 kHz, while monitoring for complete settling of electrode potential between sampling. Voltage recordings were filtered at 1 kHz. Recordings were not started until resting membrane potential had stabilized and resting membrane potential (RMP) was less than -45 mV (typically within 2 min). Somatic action potentials (APs) were generated by direct membrane depolarization with current injection through the recording electrode. The rheobase current was determined as the minimal depolarization adequate to produce an AP, and the resting voltage during this depolarization was considered the voltage threshold. AP duration was measured

at 50% resolution, whereas afterhyperpolarization (AHP) duration was measured at 80% resolution toward RMP. Excitability was assayed two ways. Examination of the firing pattern during depolarizing current injection (100 ms, 0.2 nA increments) through the recording electrode allowed categorization of neurons as either repetitively firing versus those that fire only a single AP despite depolarization (accommodation). Data were included only from neurons that generated an initial AP at 10 mV or less, and firing behavior was evaluated during additional depolarization up to 30 mV. A second, additional analysis of repetitively firing neurons examined the slope relating the number of APs evoked at different transmembrane potentials during depolarization. This frequency gain (number of APs per millivolt) was determined as a linear fit only for neurons that showed at least three different levels of firing (number of APs) at potentials <30 mV.

Patch-clamp electrophysiological recording. Voltage and currents were recorded in small- to medium-size neurons (28.8 ± 0.4 μm ; $n = 36$), using the whole-cell configuration of the patch-clamp technique at room temperature. Patch pipettes, ranging from 2 to 5 M Ω resistance, were formed from borosilicate glass (Garner Glass) and fire polished. Currents were recorded with an Axopatch 200B amplifier (Molecular Devices), filtered at 2 kHz through a 4-pole Bessel filter, and digitized at 10 kHz with a Digidata 1320 A/D interface and pClamp 9 software (Molecular Devices) for storage on a personal computer. After achieving gigaohm seal and breakthrough, membrane capacitance was determined and access resistance was compensated (60–85%). Access resistance was typically between 5 and 10 M Ω after breakthrough.

A modified Tyrode's solution was used for external bath solution, consisting of the following (in mM): 140 NaCl, 4 KCl, 2 CaCl₂, 2 MgCl₂, 10 D-glucose, 10 HEPES at pH of 7.4 adjusted with NaOH and an osmolality of 300 mOsm adjusted with sucrose. The internal pipette solution contained the following (in mM): 120 KCl, 5 Na-ATP, 0.4 Na-GTP, 10 EGTA, 2.25 CaCl₂, 5 MgCl₂, 20 HEPES at a pH of 7.2 with KOH and osmolality of 296–300 mOsm. This produced a calculated $[\text{Ca}^{2+}]_i$ of 70 nM (Maxchelator program; <http://maxchelator.stanford.edu>). A Na^+ -free/ Ca^{2+} -free external solution was prepared by removing the NaCl and CaCl₂ from the modified Tyrode's solution and adding 85 N-methyl-D-glucamine (NMDG), 0.1 EGTA, 50 tetraethylammonium (TEA), 5 4-aminopyridine.

In Ca^{2+} readdition experiments, Na^+ -free/ Ca^{2+} -free solution was applied after the whole-cell configuration was achieved, which was then changed to an identical solution to which Ca^{2+} had been added to 10 mM final concentration (Hoth and Penner, 1992). Before and after solution changes, currents were recorded during hyperpolarization steps (-100 mV for 100 ms from a holding potential of -65 mV) presented every 5 s during Ca^{2+} readdition. In a second protocol, currents were recorded during voltage ramps (-100 to $+20$ mV over 100 ms) that immediately followed a conditioning depolarization (0 mV for 500 ms) that inactivated voltage-gated Ca^{2+} channels (VGCCs). Neurons were otherwise held at a potential of -65 mV, and currents were normalized based on cell capacitance. Five traces were averaged from the baseline Na^+ -free/ Ca^{2+} -free condition compared with an average of five traces obtained after steady-state responses were achieved with readded Ca^{2+} .

Monovalent permeation experiments used a divalent-free (DVF) bath solution that was prepared by removing the CaCl₂ and MgCl₂ from the modified Tyrode's solution and adding 0.1 mM EGTA and 50 mM TEA (DeHaven et al., 2007). This solution was applied after the whole-cell configuration was achieved, in alternation with a solution that differed only in having 10 mM CaCl₂. Current was recorded while neurons were continuously hyperpolarized (-100 mV). Baseline current was determined from the initial recording (0–5 s) and subtracted from subsequent recording for each neuron. Responses to application of DVF solution and DVF containing La^{3+} or Ca^{2+} were determined from averaging the trace across 10 s once a steady-state response was achieved.

Except as described above for ramp protocols, depolarization was avoided before current recordings, to avoid Ca^{2+} influx that could alter the state of Ca^{2+} stores. External solutions were administered by bath change (3.3 ml/min; bath volume, 0.7 ml). The rate of bath change, represented by the time constant of the exponential fitted to the time course of dye washout monitored photometrically, was $\tau = 21 \pm 2$ s ($n =$

7). To deplete Ca^{2+} stores and maximally activate I_{CRAC} , TG ($1 \mu\text{M}$) was applied for 7 min in the external bath after establishing whole-cell patch configuration.

Statistical analysis. Statistical analyses were performed with Statistica (StatSoft). The *t* test or one-way ANOVA was used to detect the influence of injury group on measured parameters, except for immunoblot and quantitative reverse transcriptase-PCR (rtPCR) for which the nonparametric Kruskal–Wallis test was used. Parameters determined from intracellular recordings were analyzed by two-way ANOVA to determine the effect of injury, the effect of TRIM, and their interaction. Where main effects were observed in ANOVA, either Bonferroni's *post hoc* test or Tukey's test (when all possible comparisons were considered) was used to compare relevant means, and a value of $p < 0.05$ was considered significant. Results are reported as average \pm SEM.

Results

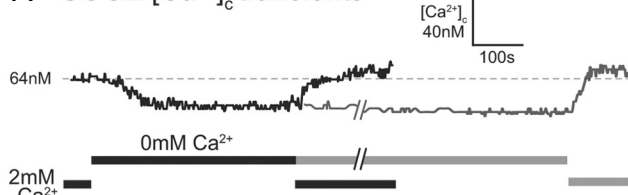
A total of 139 rats was used for the study, of which 75 were control animals and 64 were subjected to SNL. The average rate of hyperalgesia-type behavioral responses was $0.6 \pm 0.3\%$ in control animals and $41.3 \pm 2.8\%$ in SNL animals ($p < 0.001$). All SNL animals used in this study had $>20\%$ hyperalgesia responses to pin stimulation.

SOCE is present in sensory neurons

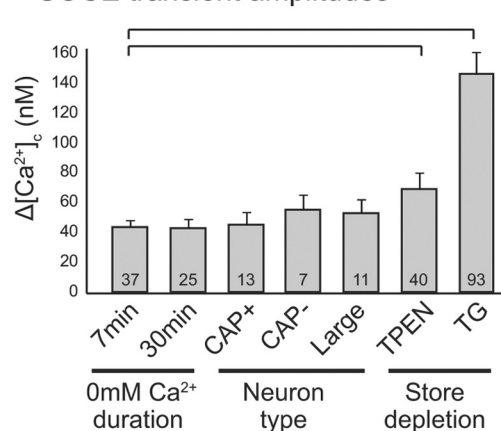
After a 7 min interval in Ca^{2+} -free bath, which is long enough to establish a stable $[\text{Ca}^{2+}]_c$ ($50 \pm 2 \text{ nM}$; $n = 57$), readdition of 2 mM bath Ca^{2+} to sensory neurons initiated Ca^{2+} influx and resulted in a rise in $[\text{Ca}^{2+}]_c$ (Fig. 1A) to levels that exceeded the original baseline in all neurons (baseline, $73 \pm 4 \text{ nM}$; readdition, $100 \pm 6 \text{ nM}$; $n = 37$; $p < 0.001$). This suggests a regulatory process driven by a signal that originates in a site other than the cytoplasm. Extension of the duration of Ca^{2+} deprivation to 30 min before Ca^{2+} readdition resulted in transients with amplitudes that did not differ from those after 7 min in Ca^{2+} -free bath (Fig. 1A,B). Sensory neurons are a heterogeneous population and include nociceptors that characteristically respond to capsaicin with Ca^{2+} influx through transient receptor potential vanilloid 1 (TRPV1) receptors (Caterina et al., 1997). The Ca^{2+} readdition transient amplitude in neurons that were subsequently shown to be sensitive to 10 nM capsaicin did not differ from those that were unresponsive to capsaicin (Fig. 1B). Large soma diameter typically characterizes fast-conducting neurons that respond to low-threshold mechanical stimuli (Waddell and Lawson, 1990). There was no difference in Ca^{2+} readdition transient amplitude between large-diameter ($39 \pm 1 \mu\text{m}$) and small-diameter ($27 \pm 1 \mu\text{m}$) neurons (Fig. 1B).

A cardinal feature of SOCE is its sensitivity to the level of intracellular Ca^{2+} stores. We therefore tested whether the Ca^{2+} readdition transient is amplified by complete depletion of ER Ca^{2+} stores achieved through exposure of neurons to the sarco-endoplasmic Ca^{2+} -ATPase (SERCA) inhibitor TG. By leaving the constitutive leak of Ca^{2+} from the ER unopposed, TG itself causes a $[\text{Ca}^{2+}]_c$ elevation that resolves within 5–7 min in Ca^{2+} -free bath (see Fig. 3A). Application of bath Ca^{2+} to neurons that had been exposed to TG ($1 \mu\text{M}$; 7 min) produced Ca^{2+} transients with amplitudes that were greater than those in other neurons without TG (Fig. 1B) ($p < 0.01$ vs control neurons). Although the amplitude of the Ca^{2+} readdition transient is a commonly accepted measure of SOCE (Usachev and Thayer, 1999; Mercer et al., 2006), it is possible that competing processes that extrude Ca^{2+} from the neuron influence the level of the steady state that underlies the $[\text{Ca}^{2+}]_c$ peak. Accordingly, we also examined the initial slope determined from the differentiated $[\text{Ca}^{2+}]_c$ trace, which may provide a more direct and valid measure of the rate of Ca^{2+} influx during bath readdition (Glitsch et al., 2002). By this

A SOCE $[\text{Ca}^{2+}]_c$ transients



B SOCE transient amplitudes



C Thapsigargin amplification

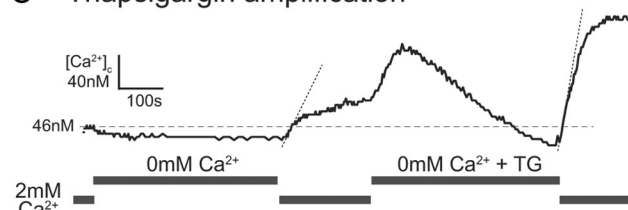


Figure 1. Manipulation of SOCE by withdrawal of Ca^{2+} from the bathing solution and the readdition of Ca^{2+} . **A**, Ca^{2+} withdrawal reduces resting $[\text{Ca}^{2+}]_c$, which is mostly complete within ~ 3 min. Withdrawal for 30 min (gray trace, $32 \mu\text{m}$ -diameter neuron) depresses $[\text{Ca}^{2+}]_c$ only slightly more than a 7 min withdrawal in a different neuron (dark trace, $30 \mu\text{m}$). Readdition of Ca^{2+} to the bath causes elevation of $[\text{Ca}^{2+}]_c$ to a level higher than the original baseline (dashed line). **B**, Amplitudes of the $[\text{Ca}^{2+}]_c$ transients induced by readdition of Ca^{2+} to the bath in separate groups of neurons. Unless otherwise indicated, neurons are small ($<34 \mu\text{m}$ diameter) and the Ca^{2+} withdrawal is for 7 min. There was no difference between bath Ca^{2+} withdrawal for 7 min versus 30 min. Neurons sensitive to capsaicin (10 nM ; Cap⁺) showed the same transient amplitude as insensitive neurons (Cap⁻). Amplitude in large neurons ($42 \pm 2 \mu\text{m}$ diameter) did not differ from small neurons. Chelation of endoplasmic reticulum Ca^{2+} stores with TPEN ($100 \mu\text{M}$; 3 min) or depletion of Ca^{2+} stores with TG ($1 \mu\text{M}$; 7 min) each increased the Ca^{2+} readdition transient amplitude. The numbers in the bars indicate number of neurons; the brackets indicate $p < 0.05$. Shown are mean \pm SEM. **C**, Trace (typical of $n = 9$) showing a greater increase in $[\text{Ca}^{2+}]_c$ with Ca^{2+} readdition to the bath solution after exposure to TG ($1 \mu\text{M}$). Additionally, the maximal rate of $[\text{Ca}^{2+}]_c$ during Ca^{2+} readdition, indicated by the tangential dotted lines, is greater after TG (3.2 nM/s) than before (1.1 nM/s).

measure, the SOCE was also greater with TG ($3.85 \pm 0.39 \text{ nM/s}$; $n = 93$) than without TG ($0.86 \pm 0.14 \text{ nM/s}$; $n = 35$; $p < 0.001$).

To confirm the influence of TG on SOCE, separate experiments were performed in which Ca^{2+} readdition transients were compared in the same neuron under baseline conditions and again after TG application (Fig. 1C). TG increased the transient amplitude 2.7 ± 0.4 -fold compared with the transient before TG ($p = 0.0001$; $n = 9$). This was significantly greater amplification ($p < 0.01$) than the slight increase in the second transient (1.2 ± 0.1 -fold; $p = \text{NS}$; $n = 24$) when Ca^{2+} readdition was repeated in the absence of TG. Measuring slopes confirmed that TG increased the Ca^{2+} influx rate 3.3 ± 1.1 -fold compared with base-

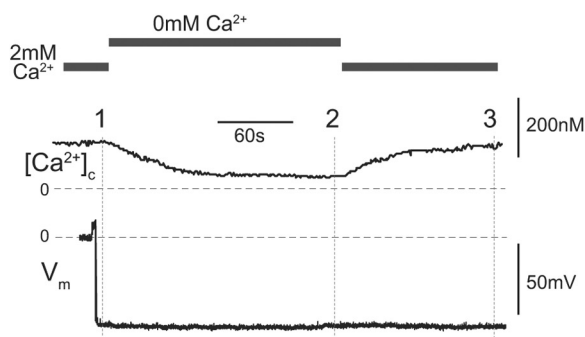
line (Fig. 1C) ($p < 0.05$; $n = 9$), whereas the amplification during repeat Ca^{2+} re-addition without TG (1.4 ± 0.1 -fold; $p < 0.01$; $n = 23$) was significantly less ($p < 0.001$).

Chelation of ER Ca^{2+} stores provides an alternative method for testing the influence of Ca^{2+} stores on Ca^{2+} influx. TPEN passes freely through membranes and only binds Ca^{2+} at micromolar concentration, thereby having a selective effect on stored Ca^{2+} . In investigations of other cell types, TPEN depresses free Ca^{2+} concentration in ER stores within 10 s of application, without an effect on cytoplasmic Ca^{2+} levels (Hofer et al., 1998). Ca^{2+} readdition to sensory neurons incubated in TPEN ($100 \mu\text{M}$; 3 min) produced transient amplitudes that were on average 1.7-fold greater ($p < 0.05$) than those in other neurons incubated in Ca^{2+} -free bath (7 min) without the chelator (Fig. 1B). Compared with TPEN, TG may have a relatively greater effect on $[\text{Ca}^{2+}]_c$ rise after bath Ca^{2+} readdition because of its blockade of Ca^{2+} sequestration from the cytoplasm via SERCA. Together, the findings from depletion and chelation of Ca^{2+} stores reveal a Ca^{2+} entry process that is regulated by the state of ER Ca^{2+} stores.

Since sensory neurons possess a variety of VGCCs, we examined the possibility that activation of these channels by membrane depolarization during Ca^{2+} readdition might underlie a component of the observed Ca^{2+} influx. Intracellular electrode recordings showed membrane potential was unchanged during withdrawal of Ca^{2+} from the bath and during subsequent Ca^{2+} readdition (Fig. 2A,B), which indicates that neither action potentials nor incremental membrane depolarization contribute to generating the Ca^{2+} readdition transient. It is possible nonetheless that Ca^{2+} may enter neurons through VGCCs that are conducting at resting membrane potential, particularly low-voltage-activated T-type Ca^{2+} channels (Lee et al., 1999). However, the presence of mibefradil (200 nM), a T-type VGCC blocker, did not alter the transient amplitude during Ca^{2+} readdition to TG-treated neurons ($1 \mu\text{M}$; 7 min) compared with a preceding Ca^{2+} readdition in the absence of mibefradil ($96 \pm 14 \text{ nM}$ baseline; $92 \pm 10 \text{ nM}$ after blockade; $p = 0.63$; $n = 14$). Combined application of selective VGCC blockers (Fig. 3A) (mibefradil, nitrendipine, $10 \mu\text{M}$, for L-type current; SNX-111, 200 nM , for N-type current; ω -conotoxin Aga-IVA, 200 nM , for P/Q-type current; SNX-482, 100 nM , for R-type current) also did not alter Ca^{2+} readdition transient amplitudes ($94 \pm 10 \text{ nM}$ baseline; $135 \pm 10 \text{ nM}$ after blockade; $p = 0.70$; $n = 32$), which suggests that no Ca^{2+} enters through this pathway and confirms Usachev and Thayer's previous findings in cultured embryonic neurons.

Sensitivity to blockers of SOCE, such as low concentrations of La^{3+} , has been used in previous studies to identify SOCE (Szikra et al., 2009). During Ca^{2+} readdition in TG-treated sensory neurons (Fig. 3B), we found a substantial suppression of transient amplitude by La^{3+} ($10 \mu\text{M}$), which eliminated $79 \pm 7\%$ of the Ca^{2+} readdition transient compared with other neurons without blocker. 2-APB ($100 \mu\text{M}$), another commonly used SOCE inhibitor (Bootman et al., 2002), moderately decreased the Ca^{2+} readdition transient amplitude in sensory neurons by $39 \pm 6\%$. TRIM ($400 \mu\text{M}$), which has been used to block SOCE in neurons (Tobin et al., 2006), suppressed the readdition transient by $61 \pm 5\%$. The

A Membrane potential during SOCE



B Data summary (n=9)

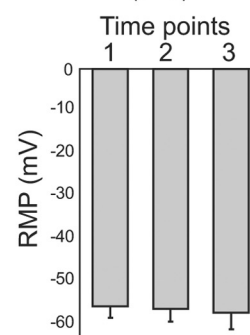


Figure 2. Membrane potential of a sensory neuron after dissociation from a dorsal root ganglion, recorded by intracellular electrode during inactivation of SOCE by bath Ca^{2+} withdrawal and SOCE activation by Ca^{2+} readdition. **A**, Sample trace from a simultaneous recording of membrane potential and $[\text{Ca}^{2+}]_c$ from a control neuron ($32 \mu\text{m}$ diameter). **B**, There is no difference in potential immediately after impalement (time point 1), during decreased $[\text{Ca}^{2+}]_c$ with Ca^{2+} withdrawal (time point 2), or on readdition of Ca^{2+} to the bath solution (time point 3). Shown are mean \pm SEM.

commonly used SOCE blocker SKF-96365 (10 – $50 \mu\text{M}$) did not have any significant effect on sensory neurons. ML-9, a novel SOCE blocker (Smyth et al., 2008), itself elevated $[\text{Ca}^{2+}]_c$ by $83 \pm 24 \text{ nM}$ ($n = 15$) in neurons bathed in Ca^{2+} -free solution, indicating release of Ca^{2+} from stores, and was not investigated further.

I_{CRAC} underlies SOCE in sensory neurons

Direct measurement of the Ca^{2+} release-activated current I_{CRAC} has been achieved in expression systems and in several native cell types. The exceptionally small conductance of store-operated Ca^{2+} channels eliminates the option of single-channel recording, so we used the whole-cell patch-clamp technique to identify I_{CRAC} .

We initially attempted to record a Ca^{2+} -dependent inward current at the approximate natural resting potential of sensory neurons (-65 mV). Ca^{2+} readdition produced small increases in inward current (Fig. 4A), but this approach produced inconsistent results, as has been reported previously (Liu et al., 2003). We therefore used voltage conditions that amplified the observable influence of extracellular Ca^{2+} . During hyperpolarization steps to -100 mV (Fig. 4B) (Hoth and Penner, 1992), I_{Ca} in bath containing 10 mM Ca^{2+} ($-1.4 \pm 0.1 \text{ pA/pF}$) was greater than the current recorded in the same neurons in bath without Ca^{2+} ($-1.0 \pm 0.1 \text{ pA/pF}$; $n = 5$; $p < 0.001$), confirming a Ca^{2+} -dependent inward current in the absence of depolarization. During ramp depolarization (Parekh, 1998; DeHaven et al., 2007), comparison of currents before and after readdition of bath Ca^{2+} to TG-treated neurons (Fig. 4C) revealed a greater current in the presence of bath Ca^{2+} ($-3.1 \pm 0.8 \text{ pA/pF}$; measured at -80 mV) than during Ca^{2+} -free conditions in the same neurons ($-0.8 \pm 0.1 \text{ pA/pF}$; $n = 5$; $p < 0.05$), again demonstrating a Ca^{2+} -dependent inward current. Inward rectification, which is a characteristic feature of I_{CRAC} (Hoth and Penner, 1992), was observed in the Ca^{2+} -dependent component of the current (Fig. 4C, subtracted current), supporting the identification of this current as I_{CRAC} .

Store-operated Ca^{2+} channels become nonselective for Ca^{2+} ions in the absence of divalent cations, whereupon a high rate of Na^{+} influx provides a more readily measurable manifestation of I_{CRAC} (Hoth and Penner, 1993; DeHaven et al., 2007). Only small currents were induced on exposure of sensory neurons to DVF bath solution under baseline conditions. However, sensory neurons incubated in TG ($1 \mu\text{M}$ for 7 min) showed robust I_{CRAC} on

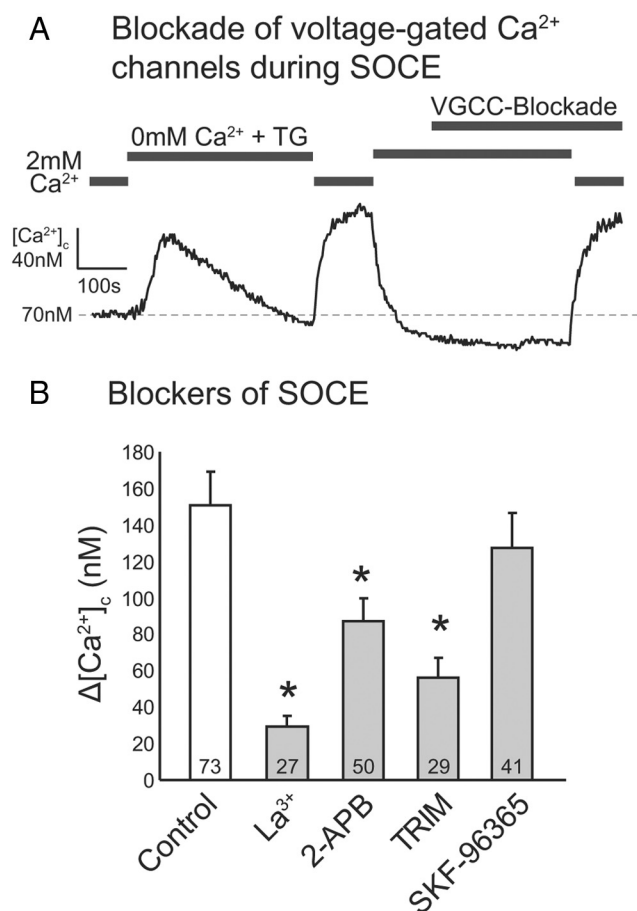


Figure 3. Effect of blockers on SOCE measured as the $[\text{Ca}^{2+}]_c$ rise on bath Ca^{2+} readdition. **A**, Blockade of VGCCs with combined administration of mibefradil (200 nM) for T-type current, nitrendipine (10 μM) for L-type current, SNX-111 (200 nM) for N-type current, ω -conotoxin Aga-IVA (200 nM) for P/Q-type current, and SNX-482 (100 nM) for R-type current does not influence the $[\text{Ca}^{2+}]_c$ increase on bath Ca^{2+} readdition in a control neuron (28 μm diameter) treated with TG (1 μM). Typical of $n = 32$. **B**, Specific blockers of SOCE reduce the amplitude of $[\text{Ca}^{2+}]_c$ rise on bath Ca^{2+} readdition. La^{3+} (10 μM), 2-APB (100 μM), and TRIM (400 μM) significantly ($*p < 0.05$) reduced transient amplitude. SKF-96365 (10–50 μM) had no effect. Shown are mean \pm SEM.

exposure to DVF conditions, unlike neurons without store depletion ($p < 0.01$ for DVF with vs without TG) (Fig. 4D,E), which identifies this as a current conducted by store-operated channels. The initiation the DVF-induced inward current showed a delay (53 ± 7 s; $n = 6$) (Fig. 4D), despite previous store depletion by incubation in TG. We attribute this delay to the time required to achieve the low level of bath Ca^{2+} that is necessary to allow nonselective conductance, for which reported K_d range from 1.7 to 4.5 μM (Lepplé-Wienhues and Cahalan, 1996; Kerschbaum and Cahalan, 1998; Rychkov et al., 2001). Specifically, an exponential model incorporating the bath volume (0.7 ml) and inflow rate (3.3 ml/min) predicts 110 and 98 s to reach these levels of bath Ca^{2+} , although imperfect mixing may cause faster washout in the central area used for recording. Sensory neurons did not show the fast depotentiation of DVF-induced I_{CRAC} as has been noted in other cells and expression systems (Zweifach and Lewis, 1996; DeHaven et al., 2007; Smyth et al., 2008). Return of Ca^{2+} to the bath resulted in immediate termination of Na^+ permeation (Fig. 4D). Additional recognition of the observed current as I_{CRAC} was obtained through the application of La^{3+} (10 μM), an established blocker of I_{CRAC} (Hoth and Penner, 1993), which elimi-

nated 62% of the current initiated by DVF solution in TG-treated neurons ($p < 0.05$ vs neurons without TG) (Fig. 4D,E).

Identification of molecular components of SOCE

STIM1 protein has previously been confirmed in neuronal tissues (Gasperini et al., 2009; Klejman et al., 2009), but not in adult sensory neurons, whereas Orai1 has been colocalized with STIM1 in brain neurons (Klejman et al., 2009). In DRG neurons, we have found expression of both components of SOCE in sensory neurons at the protein level by immunoblotting (Fig. 5A,B) and at the transcript level by quantitative rtPCR (Fig. 5C) ($n = 3$ control animals for both determinations), indicating that STIM1 and Orai1 are available in sensory neurons as potential constituents of SOCE. Immunohistochemistry of DRG tissue from control animals ($n = 3$) revealed the presence of STIM1 in neuronal somata as a homogeneous distribution in the cytoplasm (Fig. 6A), consistent with its location in the ER. There was no preferential expression of STIM1 in DRG subpopulations of different neuronal size (Fig. 6B). Double staining for STIM1 with NeuN, a neuron-specific marker (Fig. 6A), revealed expression of STIM1 in all neurons. Using glutamine synthetase as a marker for satellite glial cells (Weick et al., 2003) demonstrated that STIM1 is also present in the cytoplasm of satellite glial cells. Since available antibodies to Orai1 protein reacted with nonspecific bands in immunoblotting, immunohistochemical selectivity could not be assured and anatomic identification was not performed.

Functional role of SOCE in sensory neurons

The influence of SOCE on neuronal function is poorly defined (Putney, 2003). SOCE has been noted to modulate resting $[\text{Ca}^{2+}]_c$ in rat sympathetic neurons (Wanaverbecq et al., 2003). We found that most (57 of 71; 80%) sensory neurons responded to Ca^{2+} withdrawal with a fall in $[\text{Ca}^{2+}]_c$ (Fig. 1A) by 17 ± 3 nM ($p < 0.001$ withdrawal vs baseline) after 7 min exposure to Ca^{2+} -free bath (Fig. 7A), which indicates a dependence of resting $[\text{Ca}^{2+}]_c$ on ongoing SOCE. In a subset of neurons, we extended the interval of Ca^{2+} withdrawal to 30 min, but did not observe any significant difference compared with the 7 min interval (14 ± 2 nM; $p < 0.001$, withdrawal vs baseline; $p = 0.42$ for 7 vs 30 min).

Neurons, particularly slowly conducting C-type neurons with small-diameter somata, may remain quiescent for a sustained period of time (Schmidt et al., 1995). Since extrusion of cytoplasmic Ca^{2+} by the plasma membrane Ca^{2+} -ATPase continues in resting neurons (Wanaverbecq et al., 2003), SOCE may be an important source of Ca^{2+} influx for maintaining intracellular stores during inactivity. To test this, resting sensory neurons were incubated in Ca^{2+} -free bath solution for various time intervals and then exposed to 20 mM caffeine, which leads to a quantifiable emptying of Ca^{2+} stored in the ER (Rigaud et al., 2009). Releasable Ca^{2+} significantly decreased after 7 min in Ca^{2+} -free bath and even more after 30 min (Fig. 7B), revealing a constitutive role of SOCE in the maintenance of intraneuronal Ca^{2+} store levels.

Ca^{2+} stores in sensory neurons may be depleted through the activation of metabotropic receptors, such as those for bradykinin, ATP, and glutamate (Thayer et al., 1988; Crawford et al., 2000; Kruglikov et al., 2004), or by activation of high-affinity TRPV1 channels on the ER (Liu et al., 2003). In the absence of neuronal depolarization, the SOCE influx pathway may serve a critical role in generating plasmalemmal Ca^{2+} influx for replenishing Ca^{2+} stores. We found that Ca^{2+} stores, measured by release with caffeine (20 mM), recover almost completely during 10 min with 2 mM bath Ca^{2+} (second transient compared with first; amplitude, $89 \pm 5\%$; area, $72 \pm 3\%$; $n = 26$) (Fig. 7C), but

recovery fails in the absence of bath Ca^{2+} (amplitude, $5 \pm 2\%$; area, $3 \pm 1\%$; $n = 14$), indicating that SOCE is needed for replenishing intraneuronal Ca^{2+} stores after a release event.

Effect of painful nerve injury on SOCE

In previous studies, we found that nerve injury depresses resting $[\text{Ca}^{2+}]_c$ and diminishes Ca^{2+} stores (Fuchs et al., 2005; Gemes et al., 2009; Rigaud et al., 2009). Since our present findings show that SOCE functions to maintain intracellular levels of cytoplasmic and releasable Ca^{2+} , we examined the possibility that SOCE is deficient after peripheral nerve injury by SNL, a standard model of neuropathic pain. This proved not to be the case. The amplitude of the SOCE transient on Ca^{2+} readdition was increased in axotomized L5 neurons after SNL compared with neurons from control animals, after both 7 and 30 min of Ca^{2+} withdrawal, whereas there was no effect on adjacent L4 neurons (Fig. 8A). Analysis of the transient slope similarly showed an amplification of SOCE after injury (Fig. 8A). In contrast, when SOCE was maximized by store depletion with TG, transient amplitude and slope in injured SNL L5 neurons were no different from control neurons (Fig. 8B), implying that injured neurons have increased regulatory drive for SOCE but not increased maximal efficacy of SOCE.

To determine whether STIM1 and Orai1 expression is affected by injury, levels of protein and transcript of both genes were measured after SNL. The levels of STIM1 and Orai1 protein determined by immunoblotting were not significantly different between the DRGs of control ($n = 3$) and injured ($n = 3$) animals (STIM1, $p = 0.12$; Orai1, $p = 0.73$) (Fig. 5B). Similarly, quantitative rtPCR analysis (Fig. 5C) indicated that transcript levels of STIM1 ($p = 0.67$) and Orai1 ($p = 0.49$) in L5 DRGs of control animals ($n = 3$) and L4 and L5 DRGs of the injured animals ($n = 3$) were comparable. The anatomical distribution of STIM1 in L4 and L5 DRG sections from SNL animals ($n = 3$) double stained for STIM1 and NeuN were not different from control findings described above (Fig. 6A). These analyses together indicate that STIM1 and Orai1 expression is not altered by peripheral nerve injury.

Direct measurement of I_{CRAC} induced by DVF conditions in injured SNL L5 neurons again showed delays in onset of the current (without TG, 105 ± 21 s; $n = 8$; with TG, 77 ± 18 s; $n = 6$). In the absence of store depletion, I_{CRAC} was greater in SNL L5 neurons (-4.15 ± 0.64 pA/pF; $n = 8$) than in control neurons (-0.41 ± 0.14 pA/pF;

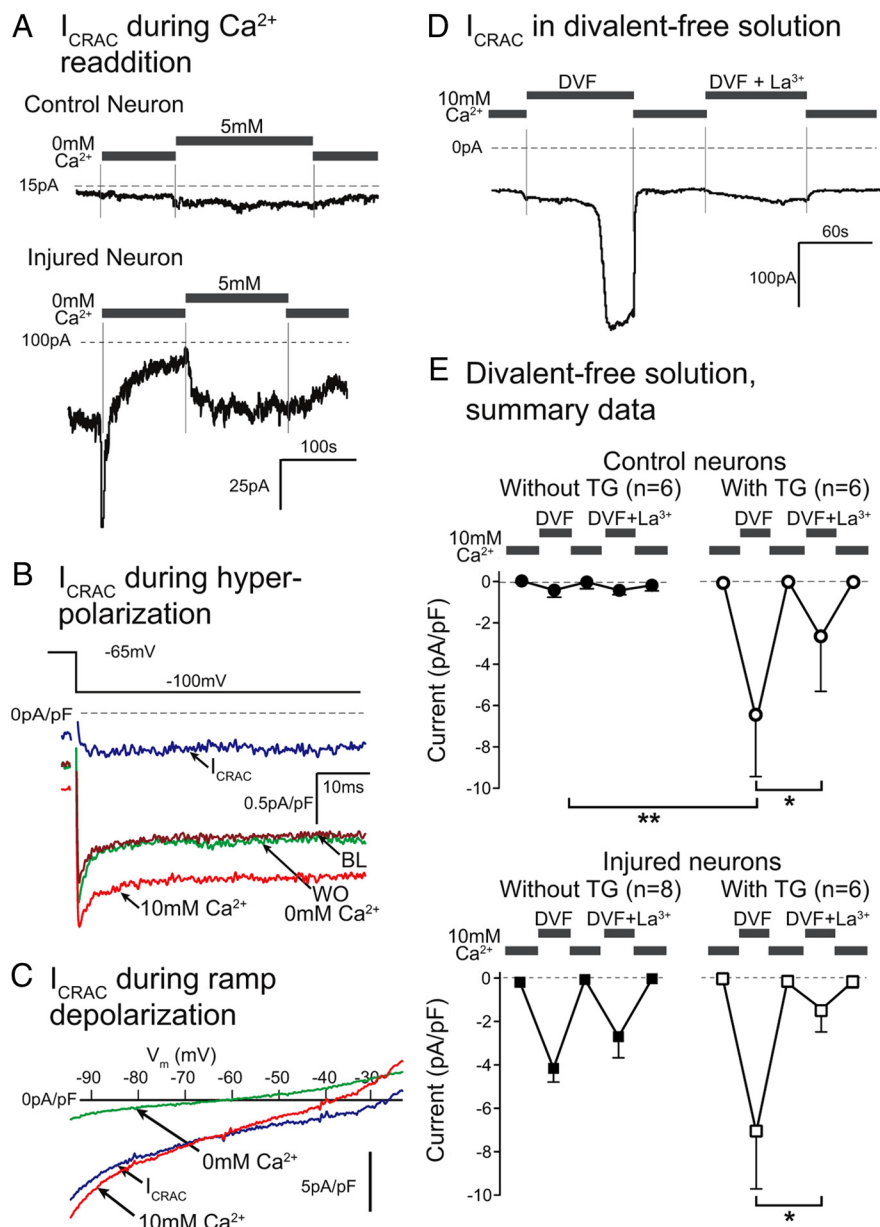


Figure 4. Recording of the Ca^{2+} release-activated current (I_{CRAC}). **A**, Withdrawal of bath Ca^{2+} lowers inward current, and readdition of bath Ca^{2+} (5 mM) elevates current during voltage clamp (-65 mV) of a control neuron (30 μm diameter; top panel) and an injured neuron (30 μm ; bottom panel) by SOCE. The scale bars apply to both traces. **B**, Current traces generated during step hyperpolarizations in a control neuron (30 μm). The baseline trace (BL) was during 0 bath Ca^{2+} . Inward current induced by hyperpolarization increased during 10 mM bath Ca^{2+} and returned to baseline levels with washout of Ca^{2+} from the bath (WO). The difference current (baseline trace subtracted from the 10 mM Ca^{2+} trace) represents I_{CRAC} . (Typical of $n = 5$.) **C**, Presentation of a ramp depolarizing voltage command (12 mV/ms) generates current (plotted here against voltage) in a control neuron (28 μm) that is less with 0 bath Ca^{2+} than during 10 mM bath Ca^{2+} . The difference trace represents I_{CRAC} . Outward current is carried by K^{+} channels that were sensitive to (data not shown), but incompletely blocked by, bath TEA (50 mM). The I_{CRAC} trace shows inward rectification, with an inflection at approximately -34 mV, above which Ca^{2+} -sensitive K^{+} current contributes an outward component. (Typical of $n = 5$.) **D**, After incubation in TG (1 μM for 7 min), exposing a control neuron (32 μm) to bath solution lacking divalent cations (DVF) produced a large inward current through the store-operated Ca^{2+} channels, which is blocked by La^{3+} (10 μM). **E**, Data from experiments such as shown in **D**. In control neurons (top panel), DVF produces minimal current under baseline conditions in the absence of store depletion (filled circles). In separate control neurons incubated in TG (open circles), DVF produces large inward currents that are blocked by La^{3+} . Injured neurons (SNL L5; bottom panel) show greater DVF-induced currents without store depletion by TG (filled squares), which are not significantly altered by TG (open squares). Shown are mean \pm SEM. * $p < 0.05$; ** $p < 0.01$.

$n = 6$; $p < 0.01$) (Fig. 4E), indicating that I_{CRAC} is increased in sensory neurons after nerve injury. TG failed to have a significant effect on measured I_{CRAC} in injured neurons (average, -7.04 ± 2.67 pA/pF; $n = 6$) (Fig. 4E), suggesting that injury itself depletes

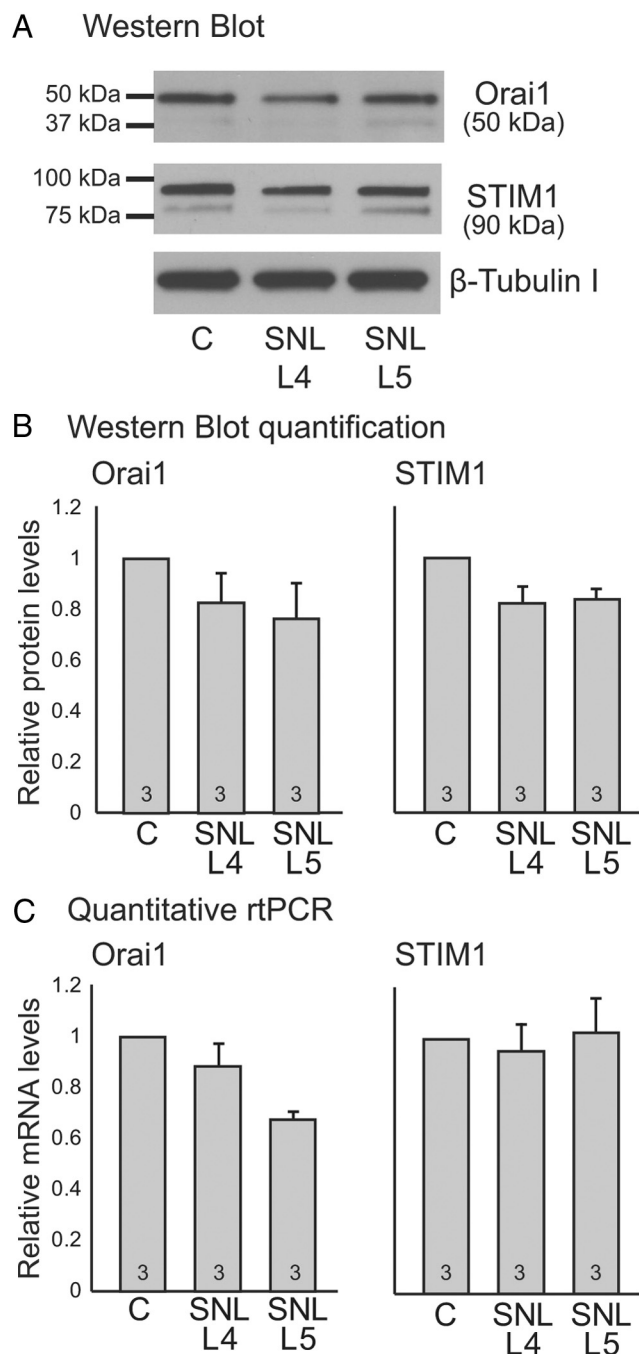


Figure 5. Identification of molecular components of store-operated Ca^{2+} channels. **A**, Western blotting detected Orai1 and STIM1 proteins in lysates from control (C) dorsal root ganglia (DRG), from fourth lumbar DRGs after fifth lumbar spinal nerve ligation (SNL L4), and from axotomized fifth lumbar DRGs after SNL (SNL L5). A dominant STIM1 band at the expected molecular weight is accompanied by a closely coherent secondary band that others have shown to be sensitive to STIM1 knockdown by RNAi (Ong et al., 2007). (Typical of $n = 3$.) **B**, Quantification of Western blots as fold difference compared with control showed no effect of injury on Orai1 and STIM1 protein levels. Shown are mean \pm SEM. **C**, Quantification of transcript levels by quantitative rtPCR also showed no effects of injury on Orai1 and STIM1 expression. For **B** and **C**, the numbers in bars indicate n .

stores and activates I_{CRAC} . After store depletion by TG, there is little difference in DVF-induced I_{CRAC} between injured neurons (-7.04 ± 2.67 pA/pF) and control neurons (-6.44 ± 1.22 pA/pF) (Fig. 4E). These findings, together with lack of effect of injury on Ca^{2+} readdition transients after TG and comparable expres-

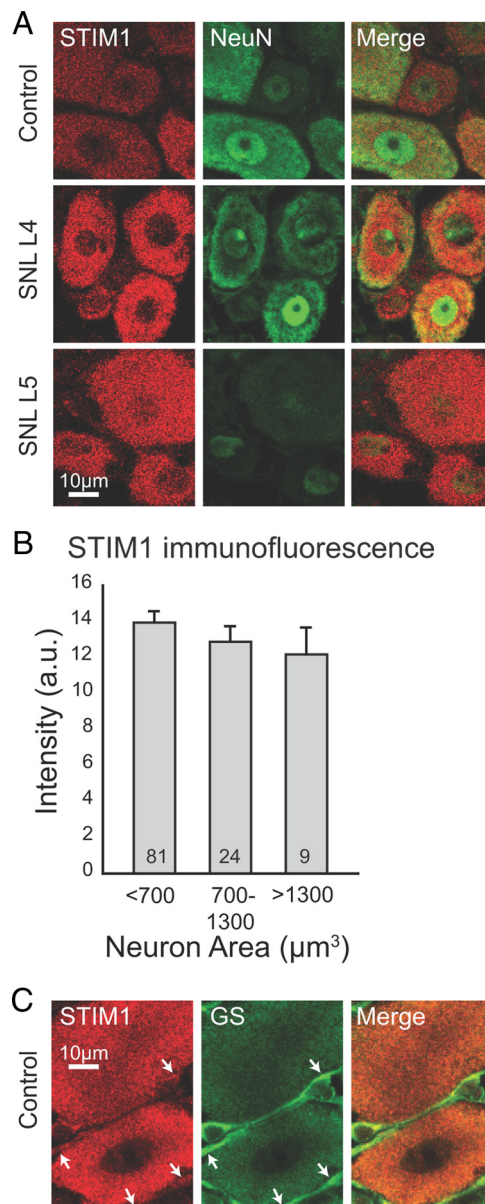


Figure 6. Immunohistochemical identification of STIM1 distribution. **A**, Staining for STIM1 (left panels) was uniformly distributed within cytoplasmic areas of cells identified as neuronal profiles through costaining with NeuN (middle panels). Only minimal nonspecific staining was present in fiber tracts. The scale bar applies to each panel. **B**, Morphometric analysis showed comparable intensity (arbitrary units, recorded using standardized image acquisition) of staining in neurons of all sizes (ANOVA, $p = 0.40$). Shown are mean \pm SEM. **C**, STIM1 (left panel) was also found in cellular components identified as satellite glial cells by their expression of glutamine synthase (GS) (middle panel). Identically placed arrows in the left and middle panels indicate cellular areas clearly identifiable as satellite glial cell cytoplasm that expresses STIM1. The scale bar applies to each panel.

sion of molecular subunits after injury, suggest that injury activates SOCE through store depletion but does not alter the intrinsic capacity of SOCE.

Injured neurons demonstrate an elevated dependence on SOCE. Although resting $[\text{Ca}^{2+}]_c$ is depressed in injured neurons (54 ± 4 nM; $n = 30$) compared with control neurons (66 ± 3 nM; $n = 57$; $p < 0.05$) and adjacent SNL L4 neurons (70 ± 3 nM; $n = 24$; $p < 0.05$), termination of SOCE by bath Ca^{2+} withdrawal imposes additional depression of $[\text{Ca}^{2+}]_c$ (Fig. 7A), provoking much lower $[\text{Ca}^{2+}]_c$ after injury in SNL L5 neurons (34 ± 2 nM)

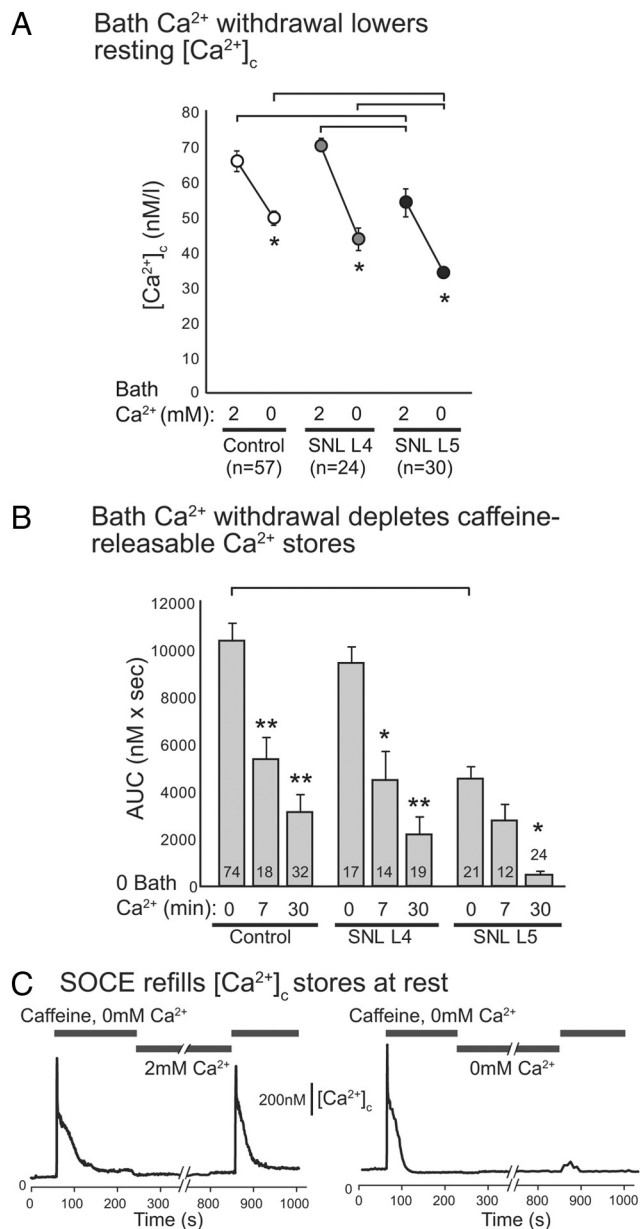


Figure 7. Functional roles of SOCE. **A**, Decreasing bath Ca^{2+} from 2 to 0 mM reduced $[\text{Ca}^{2+}]_c$ in control (C) neurons, as well as in fifth lumbar (L5) neurons axotomized by SNL and those in the adjacent L4 dorsal root ganglion (* $p < 0.05$). SNL L5 neurons had lower resting $[\text{Ca}^{2+}]_c$ levels before and after bath Ca^{2+} withdrawal compared with control and SNL L4 neurons (brackets). **B**, The size of intracellular Ca^{2+} stores that are releasable by caffeine (20 mM), measured as the area under the curve (AUC) of the caffeine-induced $[\text{Ca}^{2+}]_c$ transient, was diminished by withdrawal of bath Ca^{2+} for 7 and 30 min compared with baseline conditions (0 min of Ca^{2+} withdrawal; ANOVA main effect for time in 0 bath Ca^{2+} , $p < 0.001$; paired comparisons, * $p < 0.05$, ** $p < 0.01$). Stores are reduced in SNL L5 neurons before bath Ca^{2+} withdrawal (ANOVA main effect for injury group, $p < 0.001$; bracket indicates $p < 0.01$ for paired comparison). The numbers in the bars indicate number of neurons. Shown are mean \pm SEM. **C**, Absence of bath Ca^{2+} prevents refilling of intracellular Ca^{2+} stores. Caffeine (20 mM) releases stored Ca^{2+} in a control neuron (29 μm diameter; left panel), which is replenished during 10 min in 2 mM bath Ca^{2+} , as shown by a second caffeine-induced transient of almost equal size. In another neuron (32 μm ; right panel), absence of bath Ca^{2+} after Ca^{2+} store depletion results in a much reduced release of Ca^{2+} by the second caffeine application. The scale bar applies to both traces.

than in control conditions (50 ± 2 nM; $p < 0.001$) and SNL L4 neurons (44 ± 3 nM; $p < 0.05$). The level of stored Ca^{2+} in resting sensory neurons is also diminished by injury (Fig. 7B) (Rigaud et al., 2009). Elimination of SOCE has a particularly severe effect on

Ca^{2+} stores in injured neurons, such that SNL L5 neurons retain only 10% of their original stored Ca^{2+} after 30 min of SOCE termination through bath Ca^{2+} removal, compared with retention of 33% by control neurons and 23% by SNL L4 neurons. The combined effect of injury and SOCE termination reduces Ca^{2+} stores to 4% of that in baseline control neurons (Fig. 7B). Together, these observations indicate that SOCE plays an amplified role in maintaining Ca^{2+} homeostasis after axonal trauma in sensory neurons.

SOCE regulation of neuronal excitability

We have previously observed that blockade of Ca^{2+} -induced Ca^{2+} release (CICR) from intracellular stores increases sensory neuron excitability associated with a decreased AHP duration (Gemes et al., 2009). We therefore reasoned that store depletion from loss of SOCE might have a comparable effect. We chose not to eliminate SOCE by bath Ca^{2+} withdrawal since this can directly increase membrane excitability, independent of the loss of SOCE, by disrupting membrane charge and by decreasing depolarization-induced I_{Ca} through voltage-gated channels, which in turn decreases Ca^{2+} -activated K^{+} currents and AHPs that follow APs (Lirk et al., 2008). We instead examined the effects of SOCE blockade while recording transmembrane potentials from small- to medium-sized neurons, using an intracellular electrode technique in excised but intact DRGs that avoids the excitatory influence of neuronal dissociation (Zheng et al., 2007). Since La^{3+} is a nonselective blocker of Ca^{2+} channels including VGCCs, we therefore used TRIM (200 μM) as the best available blocker despite its incomplete efficacy (Fig. 3B). We paired recordings on each day such that an L5 DRG from a control animal was incubated in TRIM and its other L5 DRG was incubated in vehicle (0.2% DMSO) for 30 min, randomizing the sequence. For injured neurons, two L5 DRGs ipsilateral to an SNL injury were harvested from two different animals, and used in a similar paired fashion. There was no effect of TRIM on RMP or AP width (Table 1), comparable with previous findings in neurons of the supraoptic nucleus (Tobin et al., 2006). In vehicle-treated neurons, injury produced longer AP duration and decreased rheobase, as has been noted previously (Sapunar et al., 2005). TRIM increased the rheobase current necessary for initiating an AP in both control and injured neurons, and additionally decreased input resistance and lowered voltage threshold for AP generation in injured neurons. The late phase of the AHP is produced by the slow SK isoform of the Ca^{2+} -activated K^{+} channel, which is particularly dependent on Ca^{2+} released from stores. We therefore examined AHP duration, which was decreased by TRIM, particularly in injured neurons. The duration of the AHP regulates repetitive firing behavior of sensory neurons (Sapunar et al., 2005). We evaluated this by injection of suprathreshold depolarizing currents, which produced either a repetitive firing pattern (Fig. 9A) or a completely accommodating pattern in which only a single spike was generated despite depolarization beyond threshold (Fig. 9B). TRIM increased the incidence of repetitively firing neurons in both control and injured neurons. In these repetitively firing neurons, we characterized neuronal excitability further by plotting the number of evoked APs at each membrane potential, for which the slope of the fitted line represents the gain of the relationship. TRIM increased the gain in both control neurons (DMSO, 0.13 ± 0.02 APs/mV, $n = 6$; TRIM, 0.28 ± 0.06 , $n = 12$) and injured neurons (DMSO, 0.13 ± 0.02 APs/mV, $n = 6$; TRIM, 0.20 ± 0.03 , $n = 18$; ANOVA main effect of TRIM, $p < 0.01$), showing that blockade of SOCE elevates neuronal burst firing generally. Although there is a higher resting level of SOCE in

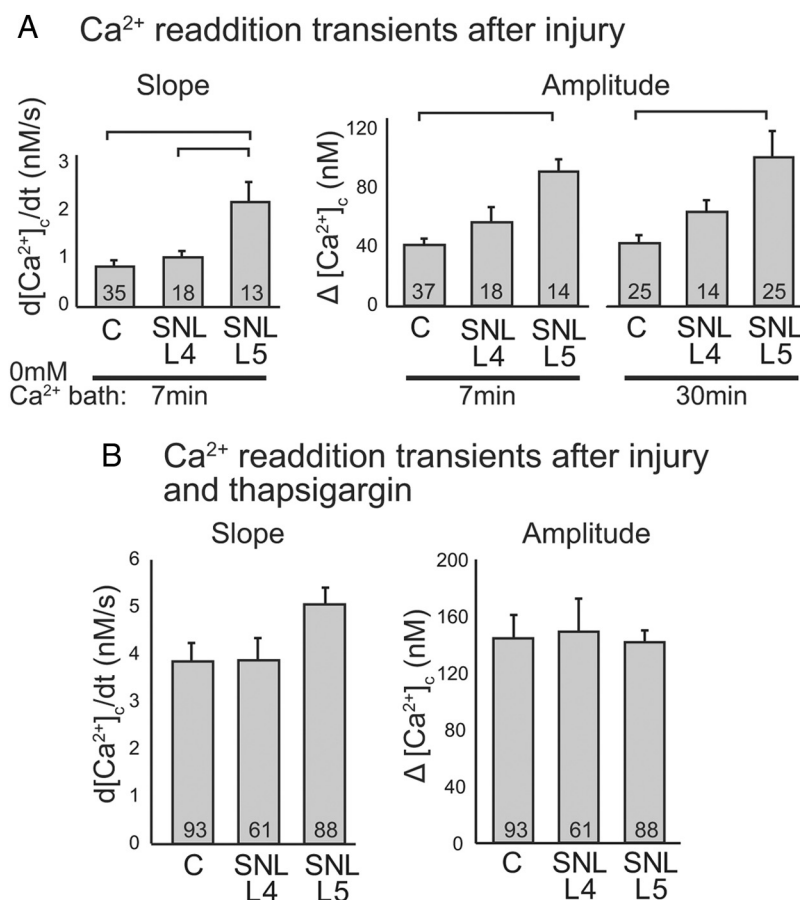


Figure 8. Effect of injury by SNL on the axotomized fifth lumbar (L5) and L4 neurons compared with control (C) neurons. **A**, Both the maximum slope of the $[\text{Ca}^{2+}]_c$ trace and the amplitude of the transient induced by Ca^{2+} readdition are increased in L5 neurons after SNL (ANOVA main effect for injury group, $p < 0.01$; bracket indicates $p < 0.05$ for paired comparison). Increasing the time of Ca^{2+} withdrawal from 7 to 30 min has no effect on the amplitude of readdition transients. **B**, Maximizing store-operated Ca^{2+} entry by store depletion with thapsigargin incubation ($1 \mu\text{M}$; 7 min) increased average transient slope and amplitude compared with transients without thapsigargin (shown in **A**) and eliminated the influence of injury because of a diminished effect on SNL L5 neurons. The numbers in the bars indicate number of neurons. Shown are mean \pm SEM.

injured neurons, we did not demonstrate a difference in the effect of TRIM on excitability of control and injured neurons, possibly because TRIM leaves 39% of SOCE intact (Fig. 3).

Apart from blocking SOCE, TRIM may also inhibit neuronal nitric oxide synthase (NOS) (Handy et al., 1995; Gibson et al., 2001), and NO may affect voltage-gated Ca^{2+} and Na^{+} currents in DRG neurons (Kim et al., 2000; Renganathan et al., 2000). We therefore examined the effect of incubating control neurons with 7-NI ($200 \mu\text{M}$; $n = 22$), a selective neuronal NOS inhibitor (Moore et al., 1993), which produced no elevation of repetitive firing compared with neurons of matched ganglia incubated in vehicle (0.1% DMSO; $n = 19$). From these findings, we infer that the increased repetitive firing of DRG neurons produced by TRIM is the result of loss of SOCE.

Influence of store depletion on depolarization-induced Ca^{2+} influx

Recent reports indicate that STIM1, when activated by store depletion, suppresses Ca^{2+} influx through L-type VGCCs (Park et al., 2010; Wang et al., 2010). To determine whether this regulatory pathway functions in sensory neurons, we incubated neurons from uninjured animals for 30 min in normal Ca^{2+} bath containing TRIM ($200 \mu\text{M}$) or vehicle (0.2% DMSO). Thereafter, the bath was changed to a solution in which Ca^{2+} was replaced by

Sr^{2+} to block SOCE, and dantrolene ($10 \mu\text{M}$) was added to block CICR from stores. After 1 min in this solution, neuronal depolarization (rapid bath application of K^{+} , 50 mM , 3 s) triggered Sr^{2+} entry through VGCCs, which produced transients in TRIM-treated neurons that had diminished amplitudes (TRIM, $0.81 \pm 0.12 R$ units, $n = 18$; DMSO, $1.08 \pm 0.08 R$ units, $n = 29$; $p < 0.05$) and initial slopes (TRIM, $0.54 \pm 0.07 R$ units/s, $n = 18$; DMSO, $0.76 \pm 0.07 R$ units/s, $n = 29$; $p < 0.05$) compared with DMSO control. These diminished transients are unlikely to be attributable to decreased CICR from TRIM-depleted stores since dantrolene will have blocked CICR in both DMSO and TRIM groups. Also, it is known that TRIM at a 10-fold higher concentration does not directly block VGCCs (Tobin et al., 2006). So, in addition to regulating SOCE, it is likely that STIM1 activation in sensory neurons inhibits VGCCs, which may in turn contribute to elevated neuronal excitability (Lirk et al., 2008).

Discussion

Our data confirm and extend previous observations that infer the presence of SOCE in central and peripheral neurons. In sensory neurons from neonatal rats, Usachev and Thayer (1999) have shown that replenishment of intracellular stores requires bath Ca^{2+} . They and others (Liu et al., 2003; Lu et al., 2006) have observed SOCE activity through the rise in $[\text{Ca}^{2+}]_c$ on return of Ca^{2+} to the bath solution, which is modulated by store level (Usachev and Thayer, 1999). We have confirmed that SOCE, represented by the readdition transient, is a general feature of acutely dissociated adult neurons, including putative nociceptors with small diameters and capsaicin sensitivity, as well as large, capsaicin-insensitive non-nociceptive neurons. Both the depletion of stores by SERCA blockade and the chelation of stores by TPEN result in amplification of the transient, suggesting the regulation of SOCE by store level. Calcium influx on return of bath Ca^{2+} cannot be attributed to currents through VGCCs or to changes in membrane potential. Although the pharmacological tools for manipulating SOCE are poorly developed, blockers that have proved successful in other reports, including La^{3+} , TRIM, and 2-APB, showed efficacy in reducing the readdition transient in sensory neurons. These observations provide strong inferential support for the existence of SOCE in sensory neurons.

We have also been able to obtain direct evidence of SOCE in neurons through the recording of I_{CRAC} . Although this current is very small at RMP, we identified an inward current component during step hyperpolarizations or ramp depolarizations that depended on the presence of external Ca^{2+} and exhibited inward rectification, which are characteristics of I_{CRAC} . The development of large inward Na^{+} flux on removal of divalent cations from the bath solution has been shown to be a typical feature of SOCE in nonexcitable cells and expression systems (Hoth and Penner,

Table 1. Electrophysiological behavior of control and injured fifth lumbar dorsal root ganglion neurons during either blockade of store-operated Ca^{2+} entry with TRIM (200 μM) or application of vehicle (DMSO, 0.2%)

	Injury group/treatment group				ANOVA main effects	
	Control		Spinal nerve ligation			
	DMSO (<i>n</i> = 23)	TRIM (<i>n</i> = 19)	DMSO (<i>n</i> = 46)	TRIM (<i>n</i> = 57)	Injury	Treatment
Diameter (μm)	30 ± 1	28 ± 1	30 ± 1	31 ± 1	NS	NS
RMP (mV)	−53.3 ± 1.9	−52.4 ± 1.9	−54.0 ± 1.0	−55.1 ± 1.1	NS	NS
<i>R</i> _{in} (MΩ)	63.1 ± 6.0	58.9 ± 10.3	99.0 ± 11.5	56.4 ± 7.3*	NS	0.002
AP duration (ms)	1.4 ± 0.2	1.2 ± 0.2	2.3 ± 0.2 [†]	2.2 ± 0.2 [†]	<0.001	NS
AHP amplitude (mV)	18.2 ± 1.1	20.0 ± 1.7	10.0 ± 0.9 [†]	12.2 ± 0.8 [†]	<0.001	0.045
AHP duration (ms)	3.6 ± 0.5	3.0 ± 0.4	4.5 ± 0.5	3.4 ± 0.2	NS	0.020
Rheobase (nA)	1.36 ± 0.15	2.37 ± 0.38*	0.78 ± 0.07	1.11 ± 0.08 [†]	<0.001	0.001
AP threshold (mV)	−12.9 ± 3.4	−12.8 ± 3.2	−19.8 ± 2.2	−30.6 ± 2.0 [†] *	<0.001	0.004
Repetitive firing (%)	26	59*	30	51*	NA	NA

RMP, Resting membrane potential; R_{in} , input resistance; AP duration, action potential width measured at 50% amplitude; AHP duration, width measured at 80% of afterhyperpolarization amplitude; rheobase, the minimum depolarizing current adequate to produce an AP; AP threshold, the minimal depolarization voltage adequate to produce an AP; repetitive firing, generation of >1 AP during depolarization to voltages <30 mV. Numbers are average \pm SEM. n , Number of neurons; NA, not applicable; NS, not significant ($p > 0.05$).

*Different from DMSO in that injury group, by paired comparisons using Tukey's honest significant difference, except for repetitive firing (t test), $p < 0.05$.

† Different from control in that treatment group.

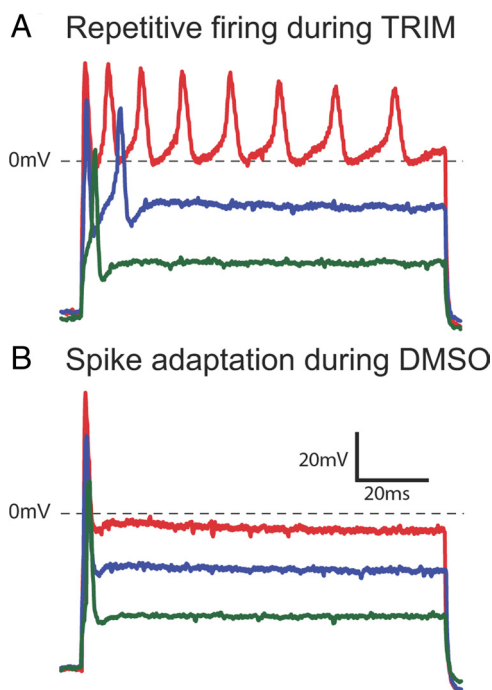


Figure 9. Effect of SOCE blockade on neuronal excitability, showing action potential generation patterns recorded by intracellular electrode in two neurons from the fifth lumbar dorsal root ganglion of rats subjected to spinal nerve ligation, during comparable depolarization (1.2, 2.4, and 3.6 nA). Noise is attributable to the use of a switching amplifier (2 kHz), used to minimize voltage error from current injection through the high-resistance electrode. **A**, Recording from a neuron (30 μm diameter) incubated with the SOCE blocker TRIM (200 μM for 45 min) shows repetitive firing during depolarization past rheobase. **B**, A different neuron (30 μm) bathed in vehicle (DMSO, 0.2%) demonstrates accommodation, with only a single action potential despite depolarization past rheobase.

1993; DeHaven et al., 2007). We observed a similar phenomenon in sensory neurons. The modulation of the DVF current by store level and bath-applied La^{3+} , an established blocker of SOCE, confirms this current as a representation of I_{CRAC} .

We additionally sought direct evidence of the presence of a SOCE mechanism in sensory neurons through identification of the molecular components underlying the process. There is now substantial agreement on the collaborative roles of STIM1 as the sensor of stored Ca^{2+} , and of Orai1 as the pore-forming protein

seated in the plasmalemma. Expression of these two proteins alone is adequate to generate SOCE, and their colocalization as puncta occurs on store depletion (Putney, 2007a,b). The involvement of canonical transient receptor potential channels (Ong et al., 2007) or the TRPV1 channel (Liu et al., 2003) in store-regulated Ca^{2+} influx has been proposed, but their participation in SOCE under the control of STIM1 is unlikely (DeHaven et al., 2009). Previous studies of neuronal tissues have identified both STIM1 and Orai1 in the brain, especially the cerebellum (Kleiman et al., 2009), and have located STIM1 in the fetal peripheral nervous system, including the DRG (Dziadek and Johnstone, 2007; Gasperini et al., 2009). Our new data demonstrate the expression of both STIM1 and Orai1 at the transcript and protein levels in adult sensory neurons, thereby establishing that the molecular hardware for SOCE activity is present in these cells. Our anatomic observations show that STIM1 is present in all neurons, with no difference in intensity between groups of differing neuronal diameter. This is consistent with our findings that SOCE is present during bath Ca^{2+} readdition in all neurons, without difference in magnitude between subgroups. We identified expression of STIM1 also in satellite glial cells. There is a growing recognition that the close apposition between the sensory neuronal soma and its surrounding satellite glial cells constitutes a functional unit (Hanani, 2005), which may also apply to Ca^{2+} signaling through a shared extracellular Ca^{2+} pool.

SOCE serves a clear purpose in nonexcitable cells such as epithelial and blood cells, by providing the dominant Ca^{2+} entry pathway for replenishing stores and for sustained elevations of $[\text{Ca}^{2+}]_i$. Identifying functional roles of SOCE in excitable cells that are equipped with high-conductance Ca^{2+} entry pathways is at an early stage. Support of the resting $[\text{Ca}^{2+}]_i$ by SOCE has been surmised from the observation of depressed $[\text{Ca}^{2+}]_i$ after removal of bath Ca^{2+} in neurons of both the central and peripheral systems (Lipscombe et al., 1989; Nohmi et al., 1992; Wanaverbecq et al., 2003; Szikra et al., 2009), which we have confirmed in adult sensory neurons. Depression of resting $[\text{Ca}^{2+}]_i$ in neurons may increase sensitivity of the TRPV1 channel (Cholewinski et al., 1993), decrease sensitivity to thermal stimuli (Guenther et al., 1999), and trigger apoptosis (Tsukamoto and Kaneko, 1993; Galli et al., 1995; Bian et al., 1997; Wei et al., 1998). We also identified a dependence on SOCE for maintenance of releasable intracellular Ca^{2+} stores and their replenishment after release, which confirms previous findings in embryonic sensory neurons (Usachev

and Thayer, 1999; Cohen and Fields, 2006). In the absence of SOCE, a quiescent neuron would potentially suffer depletion of stores, which may trigger ER stress that involves accumulation of unfolded protein, global suppression of protein synthesis, and activation of a variety of transcription factors, resulting in neuronal dysfunction and apoptosis (Paschen, 2001). Investigations of long-term potentiation in the hippocampus (Emptage et al., 2001; Baba et al., 2003) have revealed that presynaptic SOCE contributes to synaptic plasticity, so spinal cord dorsal horn plasticity may be similarly dependent on sensory neuron SOCE.

The Ca^{2+} that enters a sensory neuron during AP-induced depolarization provides membrane stabilization through the activation of Ca^{2+} -sensitive K^+ channels (Hogan et al., 2008; Lirk et al., 2008). The resulting afterhyperpolarization and diminished input resistance that follows each AP limits the impulse generation rate, or may fully eliminate repetitive firing. Release of stored Ca^{2+} (CICR) contributes to this regulation of spike frequency (Gemes et al., 2009). Additionally, data in the present report show that SOCE functions to suppress neuronal excitability. This raises the possibility that a loss of SOCE contributes to the excessive excitability noted in DRG neurons proximal to an injury (Devor and Seltzer, 1999; Sapunar et al., 2005). Our data have not supported this hypothesis. Rather, we have found that axotomized sensory neurons display amplified SOCE function under baseline conditions. However, pharmacological store depletion reveals an unchanged maximal efficacy of SOCE, and there is no evidence of altered levels of transcript or protein for STIM1 or Orai1 after injury. Combined with our previous observations of decreased releasable Ca^{2+} stores and decreased concentration of Ca^{2+} in the ER lumen after injury (Rigaud et al., 2009), our findings suggest the persistence in axotomized sensory neurons of normally functioning SOCE that is driven into a high activity state by elevated STIM1 triggered by depletion of stores.

Although a normal functioning feedback control response to store depletion satisfactorily explains elevated SOCE activity after neuronal injury, alternative mechanisms accounting for SOCE upregulation might be considered. Recent work has identified regulation of SOCE by signaling pathways involving phosphoinositides (Korzeniowski et al., 2009), tyrosine kinase, which potentiates SOCE (McElroy et al., 2009), and protein kinase C, which inhibits SOCE through phosphorylating Orai1 (Kawasaki et al., 2010), but there is no direct evidence that shifts in these factors contribute to stimulating SOCE function after injury. Ca^{2+} /calmodulin-dependent protein kinase II (CaMKII) activates SOCE (Machaca, 2003), but we have found decreased, rather than increased, CaMKII activity in sensory neurons after injury (Kawano et al., 2009; Kojundzic et al., 2010), so the increase of SOCE that we see in injured neurons occurs despite a loss of CaMKII activity.

A supportive role of SOCE in neuronal homeostasis is indicated by the pathogenic consequences of its loss. Although there has been only limited exploration in neurons, the importance of SOCE in neurological disease is highlighted by identification of diminished SOCE in neurons from mice with presenilin-1 mutations related to familial Alzheimer's disease (Yoo et al., 2000), and the direct inhibition of SOCE in hippocampal neurons by mutant presenilin-1 (Herms et al., 2003). In our present study, however, we have identified an apparent compensatory role, since SOCE is increased after injury. Although resting $[\text{Ca}^{2+}]_c$ and stores are both reduced by injury, the withdrawal of SOCE has a proportionately greater depressive effect on these factors after injury compared with the healthy state. Our data also confirm findings by others (Park et al., 2010; Wang et al., 2010) that store depletion

inhibits VGCC function, which elevates excitability in sensory neurons (Lirk et al., 2008). Therefore, supporting Ca^{2+} store levels by the concurrent activation of SOCE is particularly important so CICR can provide a means to augment the otherwise reduced activity-induced cytoplasmic Ca^{2+} signal. Our findings expose a particular dependence of injured neurons on SOCE for Ca^{2+} homeostasis and functional regulation, and highlight the utility of SOCE as a restorative mechanism.

References

- Baba A, Yasui T, Fujisawa S, Yamada RX, Yamada MK, Nishiyama N, Matsuki N, Ikegaya Y (2003) Activity-evoked capacitative Ca^{2+} entry: implications in synaptic plasticity. *J Neurosci* 23:7737–7741.
- Bian X, Hughes FM Jr, Huang Y, Cidlowski JA, Putney JW Jr (1997) Roles of cytoplasmic Ca^{2+} and intracellular Ca^{2+} stores in induction and suppression of apoptosis in S49 cells. *Am J Physiol* 272:C1241–C1249.
- Bootman MD, Collins TJ, Mackenzie L, Roderick HL, Berridge MJ, Peppiatt CM (2002) 2-Aminoethoxydiphenyl borate (2-APB) is a reliable blocker of store-operated Ca^{2+} entry but an inconsistent inhibitor of InsP3-induced Ca^{2+} release. *FASEB J* 16:1145–1150.
- Braun FJ, Broad LM, Armstrong DL, Putney JW Jr (2001) Stable activation of single Ca^{2+} release-activated Ca^{2+} channels in divalent cation-free solutions. *J Biol Chem* 276:1063–1070.
- Caterina MJ, Schumacher MA, Tominaga M, Rosen TA, Levine JD, Julius D (1997) The capsaicin receptor: a heat-activated ion channel in the pain pathway. *Nature* 389:816–824.
- Cholewinski A, Burgess GM, Bevan S (1993) The role of calcium in capsaicin-induced desensitization in rat cultured dorsal root ganglion neurons. *Neuroscience* 55:1015–1023.
- Cohen JE, Fields RD (2006) CaMKII inactivation by extracellular Ca^{2+} depletion in dorsal root ganglion neurons. *Cell Calcium* 39:445–454.
- Crawford JH, Wainwright A, Heavens R, Pollock J, Martin DJ, Scott RH, Seabrook GR (2000) Mobilisation of intracellular Ca^{2+} by mGluR5 metabotropic glutamate receptor activation in neonatal rat cultured dorsal root ganglia neurones. *Neuropharmacology* 39:621–630.
- DeHaven WI, Smyth JT, Boyles RR, Putney JW Jr (2007) Calcium inhibition and calcium potentiation of Orai1, Orai2, and Orai3 calcium release-activated calcium channels. *J Biol Chem* 282:17548–17556.
- DeHaven WI, Jones BF, Petranka JG, Smyth JT, Tomita T, Bird GS, Putney JW Jr (2009) TRPC channels function independently of STIM1 and Orai1. *J Physiol* 587:2275–2298.
- Devor M, Seltzer Z (1999) Pathology of damaged nerves in relation to chronic pain. In: *Textbook of pain*, Ed 4 (Wall PD, Melzack R, eds), pp 129–164. Edinburgh: Churchill Livingstone.
- Dziadek MA, Johnstone LS (2007) Biochemical properties and cellular localisation of STIM proteins. *Cell Calcium* 42:123–132.
- Emptage NJ, Reid CA, Fine A (2001) Calcium stores in hippocampal synaptic boutons mediate short-term plasticity, store-operated Ca^{2+} entry, and spontaneous transmitter release. *Neuron* 29:197–208.
- Fuchs A, Lirk P, Stucky C, Abram SE, Hogan QH (2005) Painful nerve injury decreases resting cytosolic calcium concentrations in sensory neurons of rats. *Anesthesiology* 102:1217–1225.
- Fuchs A, Rigaud M, Hogan QH (2007) Painful nerve injury shortens the intracellular Ca^{2+} signal in axotomized sensory neurons of rats. *Anesthesiology* 107:106–116.
- Galli C, Meucci O, Scorziello A, Werge TM, Calissano P, Schettini G (1995) Apoptosis in cerebellar granule cells is blocked by high KCl , forskolin, and IGF-1 through distinct mechanisms of action: the involvement of intracellular calcium and RNA synthesis. *J Neurosci* 15:1172–1179.
- Gasperini R, Choi-Lundberg D, Thompson MJ, Mitchell CB, Foa L (2009) Homer regulates calcium signalling in growth cone turning. *Neural Dev* 4:29.
- Gemes G, Rigaud M, Weyker PD, Abram SE, Weihrauch D, Poroli M, Zoga V, Hogan QH (2009) Depletion of calcium stores in injured sensory neurons: anatomic and functional correlates. *Anesthesiology* 111:393–405.
- Ghosh A, Greenberg ME (1995) Calcium signaling in neurons: molecular mechanisms and cellular consequences. *Science* 268:239–247.
- Gibson A, Fernandes F, Wallace P, McFadzean I (2001) Selective inhibition of thapsigargin-induced contraction and capacitative calcium entry in mouse anococcygeus by trifluoromethylphenylimidazole (TRIM). *Br J Pharmacol* 134:233–236.

- Glitsch MD, Bakowski D, Parekh AB (2002) Store-operated Ca^{2+} entry depends on mitochondrial Ca^{2+} uptake. *EMBO J* 21:6744–6754.
- Gryniewicz G, Poenie M, Tsien RY (1985) A new generation of Ca^{2+} indicators with greatly improved fluorescence properties. *J Biol Chem* 260:3440–3450.
- Guenther S, Reeh PW, Kress M (1999) Rises in $[\text{Ca}^{2+}]_i$ mediate capsaicin- and proton-induced heat sensitization of rat primary nociceptive neurons. *Eur J Neurosci* 11:3143–3150.
- Hanani M (2005) Satellite glial cells in sensory ganglia: from form to function. *Brain Res Brain Res Rev* 48:457–476.
- Handy RL, Wallace P, Gaffen ZA, Whitehead KJ, Moore PK (1995) The antinociceptive effect of 1-(2-trifluoromethylphenyl)imidazole (TRIM), a potent inhibitor of neuronal nitric oxide synthase in vitro, in the mouse. *Br J Pharmacol* 116:2349–2350.
- Hermes J, Schneider I, Dewachter I, Caluwaerts N, Kretschmar H, Van Leuven F (2003) Capacitive calcium entry is directly attenuated by mutant presenilin-1, independent of the expression of the amyloid precursor protein. *J Biol Chem* 278:2484–2489.
- Hofer AM, Fasolato C, Pozzan T (1998) Capacitative Ca^{2+} entry is closely linked to the filling state of internal Ca^{2+} stores: a study using simultaneous measurements of I_{CRAC} and intraluminal $[\text{Ca}^{2+}]$. *J Cell Biol* 140:325–334.
- Hogan Q, Sapunar D, Modric-Jednacak K, McCallum JB (2004) Detection of neuropathic pain in a rat model of peripheral nerve injury. *Anesthesiology* 101:476–487.
- Hogan Q, Lirk P, Poroli M, Rigaud M, Fuchs A, Fillip P, Ljubkovic M, Gemes G, Sapunar D (2008) Restoration of calcium influx corrects membrane hyperexcitability in injured rat dorsal root ganglion neurons. *Anesth Analg* 107:1045–1051.
- Hoth M, Penner R (1992) Depletion of intracellular calcium stores activates a calcium current in mast cells. *Nature* 355:353–356.
- Hoth M, Penner R (1993) Calcium release-activated calcium current in rat mast cells. *J Physiol* 465:359–386.
- Kawano T, Zoga V, Gemes G, McCallum JB, Wu HE, Pravdic D, Liang MY, Kwok WM, Hogan Q, Sarantopoulos C (2009) Suppressed $\text{Ca}^{2+}/\text{CaM}/\text{CaMKII}$ -dependent K_{ATP} channel activity in primary afferent neurons mediates hyperalgesia after axotomy. *Proc Natl Acad Sci U S A* 106:8725–8730.
- Kawasaki T, Ueyama T, Lange I, Feske S, Saito N (2010) Protein kinase C-induced phosphorylation of Orai1 regulates the intracellular Ca^{2+} level via the store-operated Ca^{2+} channel. *J Biol Chem* 285:25720–25730.
- Kerschbaum HH, Cahalan MD (1998) Monovalent permeability, rectification, and ionic block of store-operated calcium channels in Jurkat T lymphocytes. *J Gen Physiol* 111:521–537.
- Kim SH, Chung JM (1992) An experimental model for peripheral neuropathy produced by segmental spinal nerve ligation in the rat. *Pain* 50:355–363.
- Kim SJ, Song SK, Kim J (2000) Inhibitory effect of nitric oxide on voltage-dependent calcium currents in rat dorsal root ganglion cells. *Biochem Biophys Res Commun* 271:509–514.
- Klejman ME, Gruszczynska-Biegala J, Skibinska-Kijek A, Wisniewska MB, Misztal K, Blazejczyk M, Bojarski L, Kuznicki J (2009) Expression of STIM1 in brain and puncta-like co-localization of STIM1 and ORAI1 on depletion of Ca^{2+} store in neurons. *Neurochem Int* 54:49–55.
- Kojundzic SL, Puljak L, Hogan Q, Sapunar D (2010) Depression of $\text{Ca}^{2+}/\text{calmodulin}$ -dependent protein kinase II in dorsal root ganglion neurons after spinal nerve ligation. *J Comp Neurol* 518:64–74.
- Korzeniowski MK, Popovic MA, Szentpetery Z, Varnai P, Stojilkovic SS, Balla T (2009) Dependence of STIM1/Orai1-mediated calcium entry on plasma membrane phosphoinositides. *J Biol Chem* 284:21027–21035.
- Kruglikov I, Gryshchenko O, Shutov L, Kostyuk E, Kostyuk P, Voitenko N (2004) Diabetes-induced abnormalities in ER calcium mobilization in primary and secondary nociceptive neurons. *Pflugers Arch* 448:395–401.
- Lee JH, Daud AN, Cribbs LL, Lacerda AE, Pereverzev A, Klöckner U, Schneider T, Perez-Reyes E (1999) Cloning and expression of a novel member of the low voltage-activated T-type calcium channel family. *J Neurosci* 19:1912–1921.
- Lepple-Wienhues A, Cahalan MD (1996) Conductance and permeation of monovalent cations through depletion-activated Ca^{2+} channels (I_{CRAC}) in Jurkat T cells. *Biophys J* 71:787–794.
- Lipscombe D, Kongsamut S, Tsien RW (1989) Alpha-adrenergic inhibition of sympathetic neurotransmitter release mediated by modulation of N-type calcium-channel gating. *Nature* 340:639–642.
- Lirk P, Poroli M, Rigaud M, Fuchs A, Fillip P, Huang CY, Ljubkovic M, Sapunar D, Hogan Q (2008) Modulators of calcium influx regulate membrane excitability in rat dorsal root ganglion neurons. *Anesth Analg* 107:673–685.
- Liu M, Liu MC, Magoulas C, Priestley JV, Willmott NJ (2003) Versatile regulation of cytosolic Ca^{2+} by vanilloid receptor I in rat dorsal root ganglion neurons. *J Biol Chem* 278:5462–5472.
- Lu SG, Gold MS (2008) Inflammation-induced increase in evoked calcium transients in subpopulations of rat dorsal root ganglion neurons. *Neuroscience* 153:279–288.
- Lu SG, Zhang X, Gold MS (2006) Intracellular calcium regulation among subpopulations of rat dorsal root ganglion neurons. *J Physiol* 577:169–190.
- Machaca K (2003) Ca^{2+} -calmodulin-dependent protein kinase II potentiates store-operated Ca^{2+} current. *J Biol Chem* 278:33730–33737.
- McElroy SP, Drummond RM, Gurney AM (2009) Regulation of store-operated Ca^{2+} entry in pulmonary artery smooth muscle cells. *Cell Calcium* 46:99–106.
- Merker JC, Dehaven WI, Smyth JT, Wedel B, Boyles RR, Bird GS, Putney JW Jr (2006) Large store-operated calcium selective currents due to co-expression of Orai1 or Orai2 with the intracellular calcium sensor, Stim1. *J Biol Chem* 281:24979–24990.
- Moore PK, Babbedge RC, Wallace P, Gaffen ZA, Hart SL (1993) 7-Nitroindazole, an inhibitor of nitric oxide synthase, exhibits anti-nociceptive activity in the mouse without increasing blood pressure. *Br J Pharmacol* 108:296–297.
- Nohmi M, Hua SY, Kuba K (1992) Basal Ca^{2+} and the oscillation of Ca^{2+} in caffeine-treated bullfrog sympathetic neurones. *J Physiol* 450:513–528.
- Ong HL, Cheng KT, Liu X, Bandyopadhyay BC, Paria BC, Soboloff J, Pani B, Gwack Y, Srikanth S, Singh BB, Gill D, Ambudkar IS (2007) Dynamic assembly of TRPC1-STIM1-Orai1 ternary complex is involved in store-operated calcium influx. Evidence for similarities in store-operated and calcium release-activated calcium channel components. *J Biol Chem* 282:9105–9116.
- Parekh AB (1998) Slow feedback inhibition of calcium release-activated calcium current by calcium entry. *J Biol Chem* 273:14925–14932.
- Park CY, Shcheglovitov A, Dolmetsch R (2010) The CRAC channel activator STIM1 binds and inhibits L-type voltage-gated calcium channels. *Science* 330:101–105.
- Paschen W (2001) Dependence of vital cell function on endoplasmic reticulum calcium levels: implications for the mechanisms underlying neuronal cell injury in different pathological states. *Cell Calcium* 29:1–11.
- Putney JW Jr (2001) Pharmacology of capacitative calcium entry. *Mol Interv* 1:84–94.
- Putney JW Jr (2003) Capacitative calcium entry in the nervous system. *Cell Calcium* 34:339–344.
- Putney JW Jr (2007a) New molecular players in capacitative Ca^{2+} entry. *J Cell Sci* 120:1959–1965.
- Putney JW Jr (2007b) Recent breakthroughs in the molecular mechanism of capacitative calcium entry (with thoughts on how we got here). *Cell Calcium* 42:103–110.
- Renganathan M, Cummins TR, Hormuzdiar WN, Black JA, Waxman SG (2000) Nitric oxide is an autocrine regulator of Na^{+} currents in axotomized C-type DRG neurons. *J Neurophysiol* 83:2431–2442.
- Rigaud M, Gemes G, Weyker PD, Cruikshank JM, Kawano T, Wu HE, Hogan QH (2009) Axotomy depletes intracellular calcium stores in primary sensory neurons. *Anesthesiology* 111:381–392.
- Rychkov G, Brereton HM, Harland ML, Barritt GJ (2001) Plasma membrane Ca^{2+} release-activated Ca^{2+} channels with a high selectivity for Ca^{2+} identified by patch-clamp recording in rat liver cells. *Hepatology* 33:938–947.
- Sapunar D, Ljubkovic M, Lirk P, McCallum JB, Hogan QH (2005) Distinct membrane effects of spinal nerve ligation on injured and adjacent dorsal root ganglion neurons in rats. *Anesthesiology* 103:360–376.
- Schmidt R, Schmelz M, Forster C, Ringkamp M, Torebjörk E, Handwerker H (1995) Novel classes of responsive and unresponsive C nociceptors in human skin. *J Neurosci* 15:333–341.
- Scott BS, Edwards BA (1980) Electric membrane properties of adult mouse DRG neurons and the effect of culture duration. *J Neurobiol* 11:291–301.
- Smyth JT, Dehaven WI, Bird GS, Putney JW Jr (2008) Ca^{2+} -store-

- dependent and -independent reversal of Stim1 localization and function. *J Cell Sci* 121:762–772.
- Stathopoulos PB, Li GY, Plevin MJ, Ames JB, Ikura M (2006) Stored Ca^{2+} depletion-induced oligomerization of stromal interaction molecule 1 (STIM1) via the EF-SAM region: an initiation mechanism for capacitive Ca^{2+} entry. *J Biol Chem* 281:35855–35862.
- Szikra T, Barabas P, Bartoletti TM, Huang W, Akopian A, Thoreson WB, Krizaj D (2009) Calcium homeostasis and cone signaling are regulated by interactions between calcium stores and plasma membrane ion channels. *PLoS One* 4:e6723.
- Thayer SA, Perney TM, Miller RJ (1988) Regulation of calcium homeostasis in sensory neurons by bradykinin. *J Neurosci* 8:4089–4097.
- Tobin V, Gouty LA, Moos FC, Desarménien MG (2006) A store-operated current (SOC) mediates oxytocin autocontrol in the developing rat hypothalamus. *Eur J Neurosci* 24:400–404.
- Tsukamoto A, Kaneko Y (1993) Thapsigargin, a Ca^{2+} -ATPase inhibitor, depletes the intracellular Ca^{2+} pool and induces apoptosis in human hepatoma cells. *Cell Biol Int* 17:969–970.
- Usachev YM, Thayer SA (1999) Ca^{2+} influx in resting rat sensory neurones that regulates and is regulated by ryanodine-sensitive Ca^{2+} stores. *J Physiol* 519:115–130.
- Waddell PJ, Lawson SN (1990) Electrophysiological properties of subpopulations of rat dorsal root ganglion neurons in vitro. *Neuroscience* 36:811–822.
- Wanaverbecq N, Marsh SJ, Al-Qatari M, Brown DA (2003) The plasma membrane calcium-ATPase as a major mechanism for intracellular calcium regulation in neurones from the rat superior cervical ganglion. *J Physiol* 550:83–101.
- Wang Y, Deng X, Mancarella S, Hendron E, Eguchi S, Soboloff J, Tang XD, Gill DL (2010) The calcium store sensor, STIM1, reciprocally controls Orai and $\text{CaV}1.2$ channels. *Science* 330:105–109.
- Wei H, Wei W, Bredesen DE, Perry DC (1998) Bcl-2 protects against apoptosis in neuronal cell line caused by thapsigargin-induced depletion of intracellular calcium stores. *J Neurochem* 70:2305–2314.
- Weick M, Cherkas PS, Härtig W, Pannicke T, Uckermann O, Bringmann A, Tal M, Reichenbach A, Hanani M (2003) P2 receptors in satellite glial cells in trigeminal ganglia of mice. *Neuroscience* 120:969–977.
- Wu HE, Gemes G, Zoga V, Kawano T, Hogan QH (2010) Learned avoidance from noxious mechanical stimulation but not threshold Semmes Weinstein filament stimulation after nerve injury in rats. *J Pain* 11:280–286.
- Yoo AS, Cheng I, Chung S, Grenfell TZ, Lee H, Pack-Chung E, Handler M, Shen J, Xia W, Tesco G, Saunders AJ, Ding K, Frosch MP, Tanzi RE, Kim TW (2000) Presenilin-mediated modulation of capacitative calcium entry. *Neuron* 27:561–572.
- Zheng JH, Walters ET, Song XJ (2007) Dissociation of dorsal root ganglion neurons induces hyperexcitability that is maintained by increased responsiveness to cAMP and cGMP. *J Neurophysiol* 97:15–25.
- Zweifach A, Lewis RS (1996) Calcium-dependent potentiation of store-operated calcium channels in T lymphocytes. *J Gen Physiol* 107:597–610.